

T. Beyer, O. Mawlawi, and H.H. Quick

Contents

Introduction 7
 PET/MR Design Concepts 14
 MR-Compatible PET Detectors 18
 PET/MR Methodological Pitfalls
 and Technological Challenges 21
 PET/MR Safety 24
 Summary and Conclusion 25
 References 27

Introduction

Anato-metabolic Imaging

Most people require diagnostic tests during their lifetime in order to detect a suspected malignancy, plan a therapy and follow-up on a treatment. In almost all of these cases diagnostic tests entail a single imaging examination or a series of complementary imaging exams. Non-invasive imaging is central to personalized disease management and includes imaging technologies such as Computed Tomography (CT), Single Photon Emission Computed Tomography (SPECT), Magnetic Resonance Imaging (MRI), Ultrasound (US) or Positron Emission Tomography (PET).

Each of the above imaging tests yields a wealth of information that can be separated generally into anatomical and metabolic information. Anatomical information, such as obtained from CT or US, is represented by a set of sub-mm resolution images that depict gross anatomy for organ and tissue delineation. Malignant disease is typically detected on these images by means of locally altered image contrast or by abnormal deviations from standard human anatomy. It is important to note, that anatomical changes do not necessarily relate to the onset of malignant diseases. In other words, malignant diseases are expressed as abnormal alterations of signaling or metabolic pathways that may lead to detectable anatomical changes. Therefore, anatomical imaging alone may miss diseases frequently or diagnose diseases at an advanced stage only.

PET, as a representative of nuclear medicine imaging methods, has been shown to support accurate diagnosis of malignant disease [1] as well as providing essential information for early diagnosis of neurodegenerative diseases [2] and malfunctions of the cardiovascular system [3]. However, over 90 % of all PET examinations are performed for oncology indications. PET is based on the use of trace amounts of radioactively labeled biomolecules, such as [18F]-FDG, a fluorine-18 labeled analogue to the glucose molecule, that are injected into the patient whereby the distribution of the

T. Beyer (✉)
 Center for Medical Physics and Biomedical Engineering,
 General Hospital Vienna, Medical University Vienna,
 4L Waehringer Guertel 18-20, 1090 Vienna, Austria
 e-mail: thomas.beyer@meduniwien.ac.at

O. Mawlawi
 Department of Imaging Physics,
 MD Anderson Cancer Center, Unit 1352, Houston, TX 77030, USA

H.H. Quick
 Institute of Medical Physics (IMP),
 Friedrich-Alexander-University (FAU) Erlangen-Nürnberg,
 Henkestr. 91, 91052 Erlangen, Germany

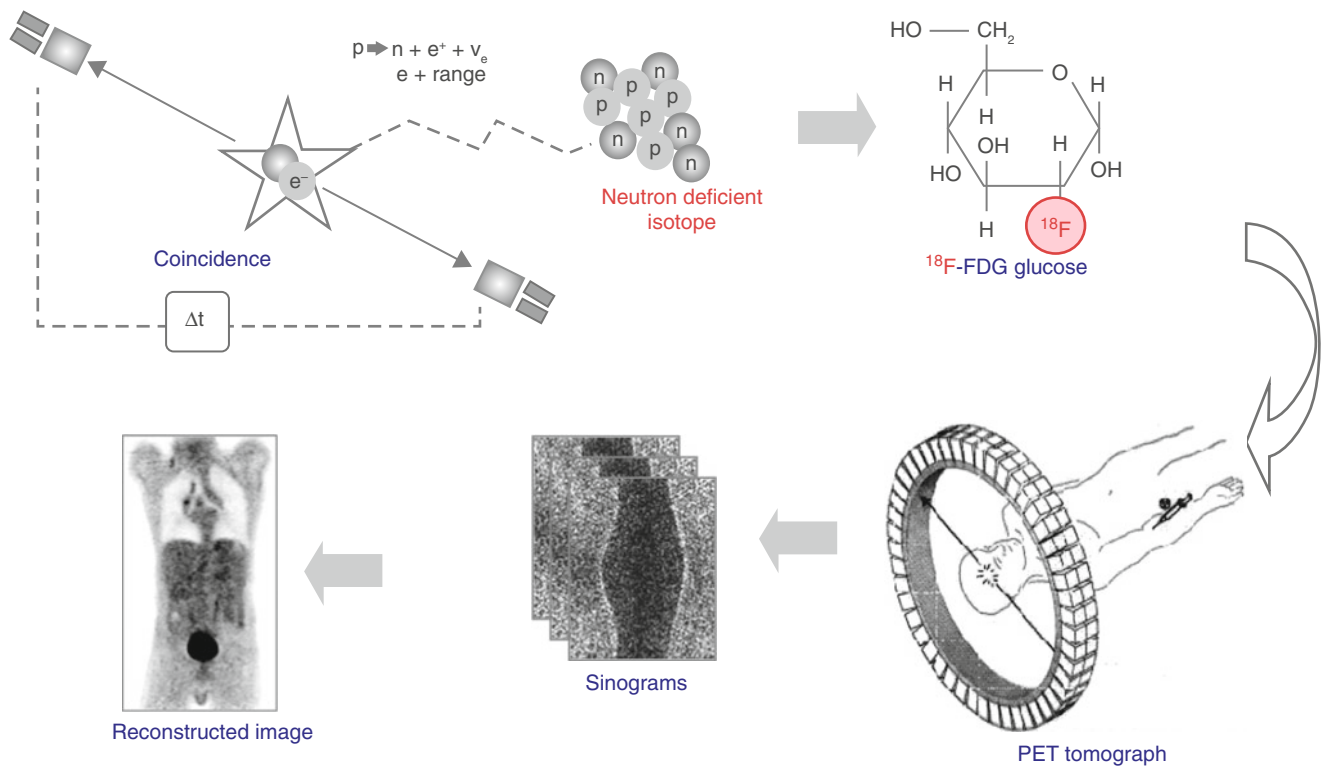


Fig. 2.1 Schematics of PET imaging: a biomolecule is labeled with a positron emitter (e.g., ^{18}F , $T_{1/2} \sim 109.8$ min) and injected into the patients. The radioactive isotope label decays by emitting a positron, which annihilates with an electron from the surrounding tissue, thus creating two

annihilation photons that are emitted back-to-back and detected by a ring of PET detectors. Image reconstruction then follows the same principles as in CT (Courtesy of David W Townsend, Singapore)

tracer is followed by detecting the annihilation photons resulting from the emission and annihilation of the positrons (Fig. 2.1).

In most cases of malignant diseases early diagnosis is key and, therefore, imaging the anatomy of a patient may not suffice in rendering a correct and timely diagnosis. Thus, medical doctors typically employ a combination of imaging techniques during the course of diagnosis and subsequent treatment to monitor their patients. Henceforth, both functional and anatomical information are essential in state-of-the-art patient management. An appreciation for this type of combined information is best illustrated with the introduction of the term “anato-metabolic imaging” [4], in reference to an ideal imaging modality that gathers both anatomical and functional information, preferably within the same examination.

Historically, medical devices to image either anatomical structure or functional processes have developed along somewhat independent paths. The recognition that combining images from different modalities can offer significant diagnostic advantages gave rise to sophisticated software techniques to co-register (aka align, fuse, superimpose) structure and function retrospectively (Fig. 2.2). The usefulness of combining anatomical and functional planar images was evident to physicians as early as in the 1960s [5]. Sophisticated image fusion software was developed from the late 1980s onwards.

For relatively rigid objects such as the brain, software can successfully align images from MR, CT and PET, whereas in more flexible environments, such as the rest of the body, accurate spatial alignment is difficult owing to the large number of possible degrees of freedom. Alternatives to software-based fusion have now become available through instrumentation that combines two complementary imaging modalities within a single system, an approach that has since been termed hardware fusion. A combined, or hybrid, tomograph such as PET/CT can acquire co-registered structural and functional information within a single study. The data are complementary allowing CT to accurately localize functional abnormalities and PET to highlight areas of abnormal metabolism.

The advantages of integrated, anato-metabolic imaging are manifold [6]. A single imaging examination provides comprehensive information on the state of a disease. Consequently, functional information is gathered and displayed in an anatomical context. Patients are invited for only one, instead of multiple exams. As shown by several groups, the combination of complementary imaging modalities can yield synergy effects for the acquisition and processing of image data [7, 8]. And, finally, experts in radiology and nuclear medicine are forced to discuss and integrate their knowledge in one report, which will perhaps be more appreciated and considered a benefit in the years to come.

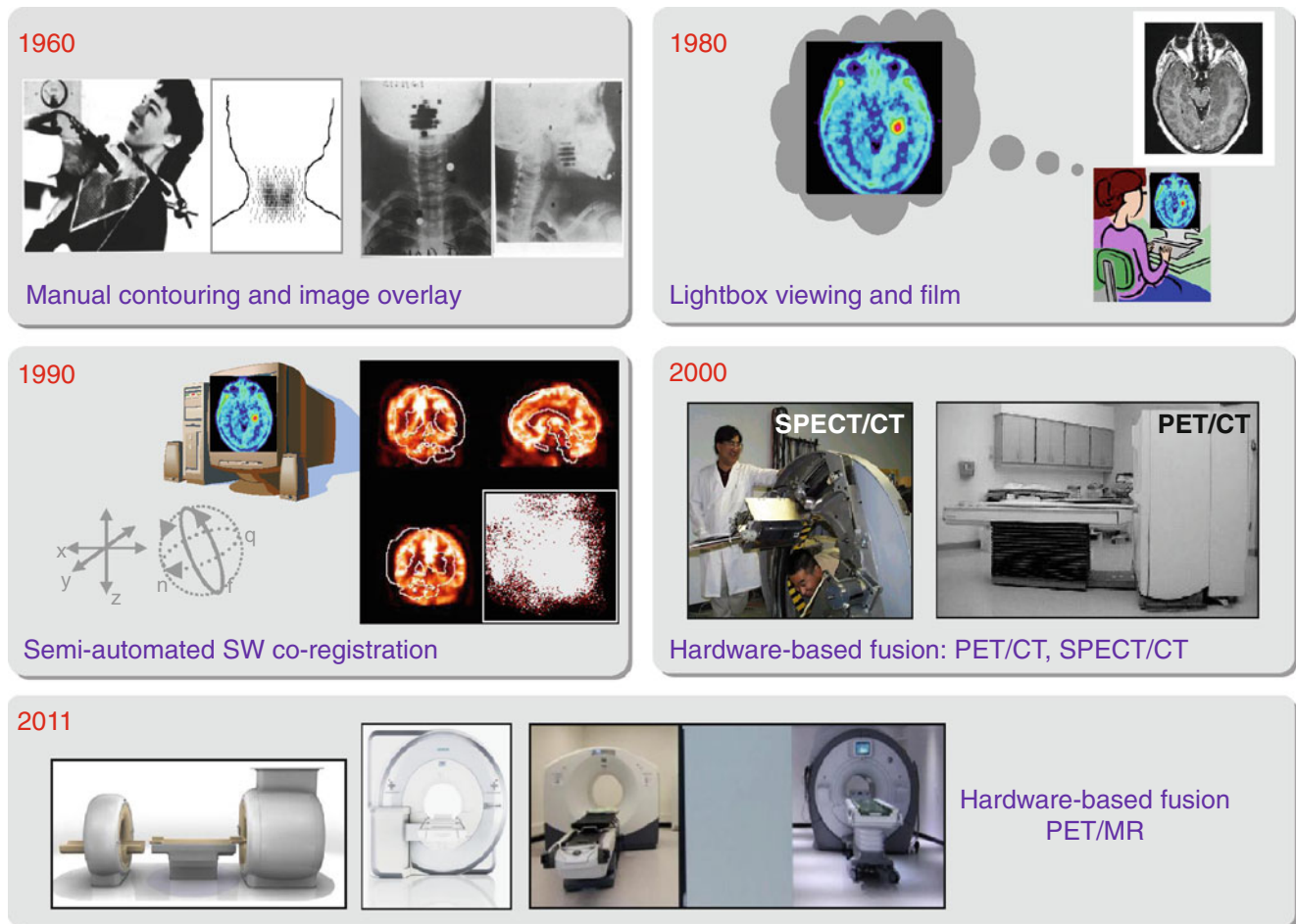


Fig. 2.2 The history of fusion imaging: from the 1960s to the 1990s complementary image information was aligned manually and later with the support of computer-based algorithms. With the introduction of pro-

totype SPECT/CT and PET/CT imaging in the 1990s and PET/MR imaging systems in the mid 2000s the field of hardware image fusion was changed dramatically

PET/CT Imaging

PET imaging has been in clinical practice since the late 1980s, thus providing valuable information in addition to CT imaging in cases where complementary diagnostic information was clinically indicated. However, the lack of fine anatomical detail in PET images may limit the localization of lesions and permit only a poor definition of lesion boundaries. This challenge was overcome by combining high-resolution anatomical CT imaging with PET, thus, providing a hardware combination for “anato-metabolic” imaging [9]. The first proposal to combine PET with CT was made in the early 1990s by Townsend, Nutt and co-workers. The foremost benefit of a PET/CT hardware combination was the intrinsic alignment of complementary image information, further supported by a clinical need at the time. A secondary benefit of this combination came with the ability to use the CT images to derive the required PET attenuation correction factors, one of the pre-requisites for quantitative PET imag-

ing [10]. CT-based attenuation correction has now become the standard in all PET/CT tomographs [11] despite the fact that some assumptions have to be made in order to transform the attenuation values of human tissues at CT energies (e.g. effective CT energies are on the order of 60–90 keV) to attenuation coefficients at the PET energy of 511 keV [12, 13]. Figure 2.3 illustrates the main drivers for PET/CT: anato-metabolic alignment and CT-based attenuation correction.

Following the introduction and validation of the first whole-body PET/CT prototype in 1998 [14] first commercial PET/CT concepts were proposed as of 2001 leading to a breadth of 25 different clinical PET/CT systems offered by six vendors worldwide in 2006. Today, four major vendors offer a range of whole-body PET/CT systems with greatly improved functionalities for both, PET and CT [15]. Table 2.1 summarizes the state-of-the-art PET/CT technology. In brief, all PET/CT systems permit total-body imaging within a single examination while using the available CT image

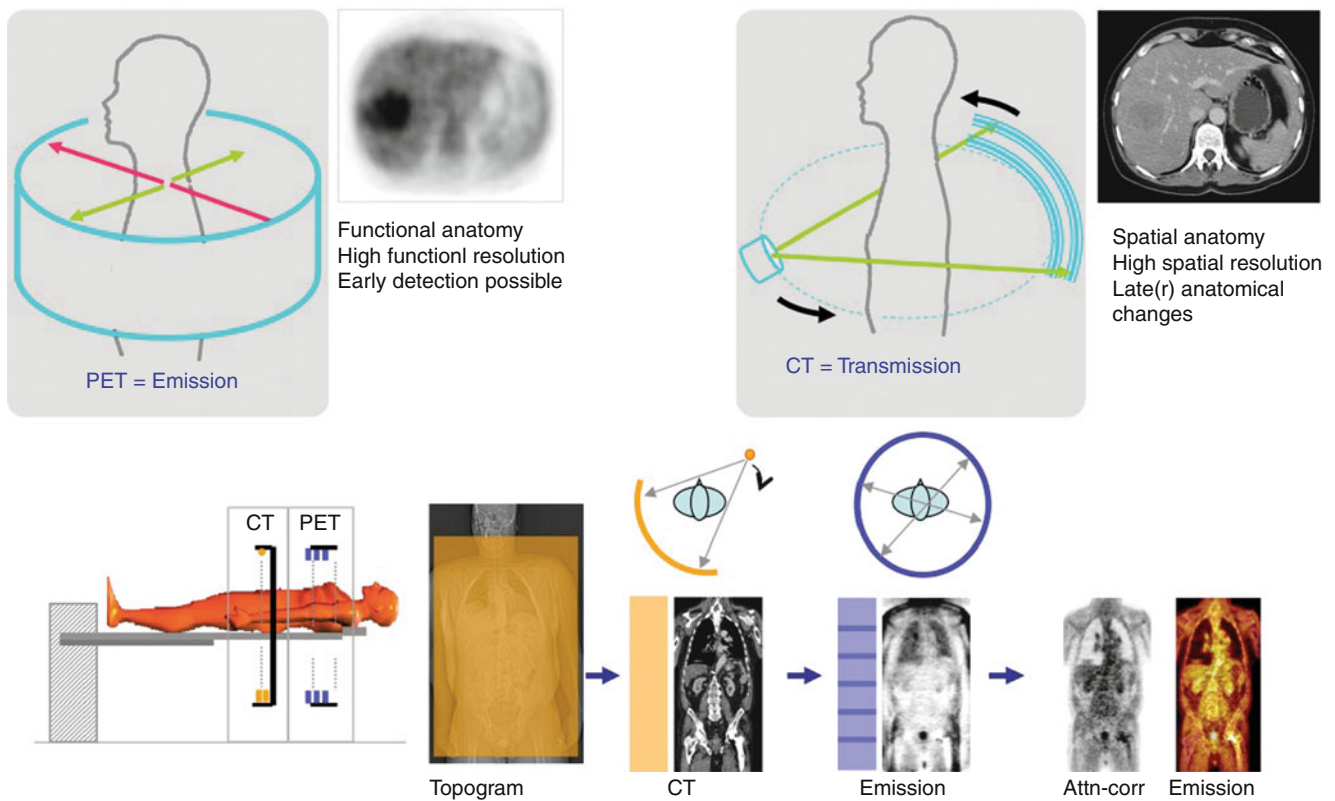


Fig. 2.3 PET and CT can be operated in close spatial proximity without cross-talk degradation of their respective performance parameters. (a) PET and CT images provide complementary diagnostic informa-

tion. (b) The use of the CT transmission images for the purpose of noiseless attenuation correction of the emission data comes as a secondary benefit of PET/CT

information for routine attenuation and scatter correction of the PET data [6]. Major technical advances include the incorporation of time-of-flight (TOF) PET acquisition mode [16], the extension of the axial field-of-view (FOV) of the PET [17] and the incorporation of system information, such as the variability of the point spread function across the field-of-view, into the reconstruction process [17].

Time-of-flight-PET was first suggested in the late 1960s in order to improve the signal-to-noise ratio (SNR) of the PET data [18]. In essence, TOF-PET requires the measurement of the arrival time of two annihilation photons arising from a given annihilation; which helps localize the origin of the annihilation (i.e. the tracer) better. TOF-PET requires fast scintillation detectors and advanced detector electronics (see also section “MR-Compatible PET Detectors”). In human studies TOF-PET can help increase the SNR by a factor of 2. Today, still few studies are available that demonstrate a significant diagnostic benefit in routine clinical applications [19, 20], but the options for trading a gain in SNR into reduced injected activities or into shorter emission scan times are available today.





Extending the axial FOV of a PET system comes at the expense of more PET detectors to be added in the axial direction. However, for a given injected activity, more

annihilation photon can be detected, thus, increasing the system sensitivity by 80 % for an additional 25 % axial coverage. This gain in sensitivity can be used for reduced emission scan times or activities injected. Despite the required increase in axial bed position overlap, the number of contiguous bed positions required to cover a given co-axial imaging range is reduced in case of PET imaging systems with an extended axial FOV.

Parallax errors arising from depth-of-interaction effects cause the spatial resolution of the PET to be a variant of the spatial location of the annihilation. If the spatial variation of the point-spread-function (PSF) is known a priori, for example, by means of standardized measurements, it can be included in the reconstruction algorithm [17, 21]. The reconstruction process becomes computationally demanding but helps improve the spatial resolution and renders the variations of the PSF in the images uniform across the field-of-view.

Over the years, the above advances have helped improve the quality and reproducibility of PET and PET/CT data (Fig. 2.4) and support a routine examination time for a standard whole-body FDG-PET/CT study of 15 min, or less, a significant advantage when compared to PET/CT imaging from a decade ago.

Table 2.1 State-of-the-art PET/CT imaging systems GE Healthcare, Philips Healthcare, Mediso and Siemens Healthcare (from left to right). The figure shows key parameters and performance measures of the PET/CT series

Discovery VCT	Ingenuity TF	AnyScan	Biograph mCT
			
CT: 16-128 slices	CT: 16-128 slices	16-slice CT	CT: 20-128
70 cm patient port	70 cm (85 cm) patient port	70 cm diameter patient port	78 cm patient port
250 kg table weight limit	215 kg table weight limit	250 kg table weight limit	250 kg table weight limit
170 cm co-scan range	190 cm co-scan range	360 cm co-scan range	170 cm co-scan range
24 rings of LYSO(Ce)	44 rings of LYSO(Ce)	24 rings of LYSO(Ce)	52 rings of LSO (Ce) crystals
4.2 x 6.3 x 25 mm ³	4.0 x 4.0 x 22 mm ³	3.9 x 3.9 x 20 mm ³	4.0 x 4.0 x 20 mm ³
Time-of-flight	Time-of-flight		Time-of-flight
15.1 cm axial FOV	18 cm axial coverage	23 cm axial coverage	21.6 cm axial coverage
70 cm transaxial FOV	67 cm transaxial FOV	55 cm transaxial FOV	70 cm transaxial FOV
PET resolution model	PET resolution model		PET resolution model
In-plane resolution: 4.9 mm	In-plane resolution: 4.7 mm	In-plane resolution: 4.1 mm	In-plane resolution: 4.4 mm
Axial resolution: 5.6 mm	Axial resolution: 4.7 mm	Axial resolution: 4.2 mm	Axial resolution: 4.4 mm
3D Sensitivity: 7.0 cps/kBq	3D Sensitivity: 7.0 cps/kBq	3D Sensitivity: 8.1 cps/kBq	3D Sensitivity: 9.7 cps/kBq
Peak NECR: 110 kcps	Peak NECR: 110 kcps	Peak NECR: 150 kcps	Peak NECR: 180 kcps
Scatter: 38% (425 keV)	Scatter: 30% (440 keV)	Scatter: 38% (425 keV)	Scatter: 33% (435 keV)
Coincidence : 4.9 ns	Coincidence : 3.8 ns	Coincidence : 5.0 ns	Coincidence : 4.1 ns
TOF resolution: 549 ps	TOF resolution: 495 ps		TOF resolution: 527 ps

Since 1998, PET/CT imaging has rapidly emerged as an important imaging tool in oncology [22], also supported by above technological advances. There is, mainly for oncology, a growing body of literature that supports the increased accuracy of staging and restaging with PET/CT compared to either CT or PET acquired separately [8]. These improvements are incremental when compared to PET, whereby PET-only demonstrates high levels of sensitivity and specificity for a wide range of disease states already. However, improvement in accuracy of PET/CT compared with PET or CT for staging and restaging is statistically significant and averages 10–15 % over all cancers [8].

Expectations Towards PET/MR

In view of the global success of PET/CT imaging with respect to both diagnostic accuracy and workflow aspects, the expectations for any new combination, such as PET/MR are very high. First and foremost, combinations of PET and MR have been discussed and prototyped since the 1990's, starting at

about the same time as PET/CT. However, while PET/CT was conceptualized based on a rather well-defined clinical need to combine functional and anatomical information from PET and CT, respectively, the developments towards an integrated PET/MR system were triggered by pre-clinical research endeavours [23]. In a well-written review of the origins of PET/MR Wehrl and colleagues reason that combined PET/MR has the potential to address major concerns in small animal imaging, such as very high exposure rates from (repeat) CT examinations and unacceptably long anesthesia times of the animals when examining them consecutive in PET and CT, or MR [24].

Almost a decade after the introduction of small animal imaging PET/MR prototype systems, industry took over that idea and presented first design concepts for clinical PET/MR systems as early as 2006. Figure 2.5 presents some key promotional factors for PET/MR in the context of the known benefits and limitations of PET/CT. First, combined PET/MR is appealing because it represents a major technological advancement. Further, assuming technical feasibility, an integrated PET/MR technology could permit simultaneous anato-metabolic

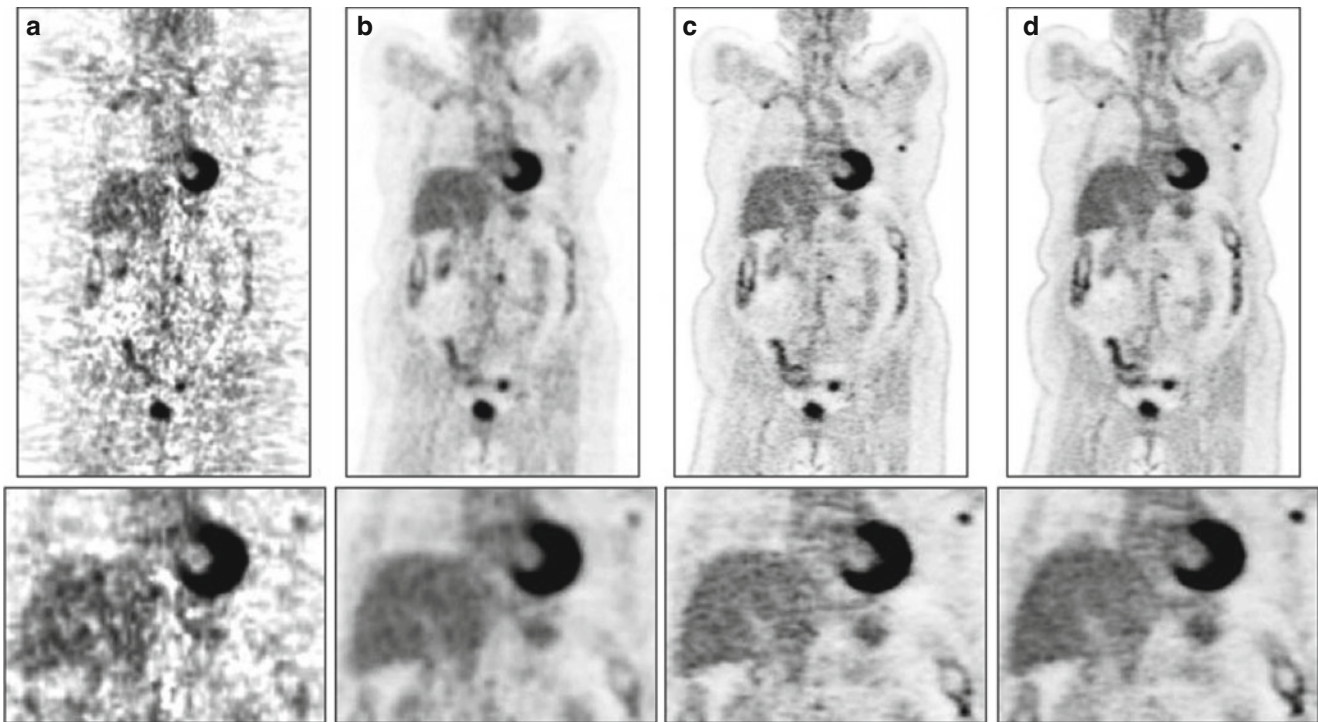
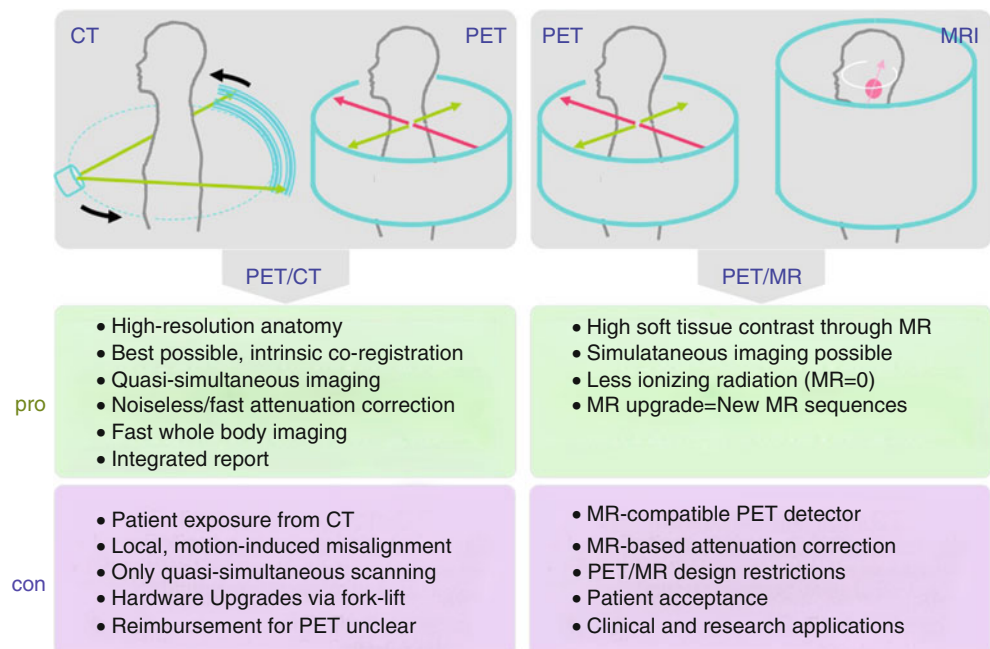


Fig. 2.4 Coronal (*top*) and transaxial (*bottom*) view of an whole-body [18F]-FDG-PET image of a patient with a BMI of 35 acquired in 3D-mode with septa retracted and reconstructed using: (a) 3D filtered back-projection algorithm with reprojection (3D-FBRP, 7 mm Gauss), (b) clinical reconstruction using FORE rebinning + 2D OSEM (8 sub-

sets, 3 iterations; 5 mm filter), (c) 3D Ordinary Poisson (OP)-OSEM with PSF reconstruction (14 subsets, 2 iterations; no smoothing), and (d) 3D OP-OSEM with both PSF and Time-of-Flight (TOF) reconstruction (14 subsets, 2 iterations, no smoothing) (Case courtesy of DW Townsend, Singapore)

Fig. 2.5 Expectations for PET/MR in the context of the existing experiences with PET/CT for patient imaging



imaging together, with the added potential of MR-based motion correction of the PET data, significantly reduced patient exposure and an increased soft tissue contrast through the use of MR instead of CT, wherever clinically indicated.

Soft tissue enhancement in MR (versus CT) may benefit the imaging of pediatric patients where normally little fatty tissues are present (Fig. 2.6), as well as for studying patients for indications related to the brain, parenchymal organs or the

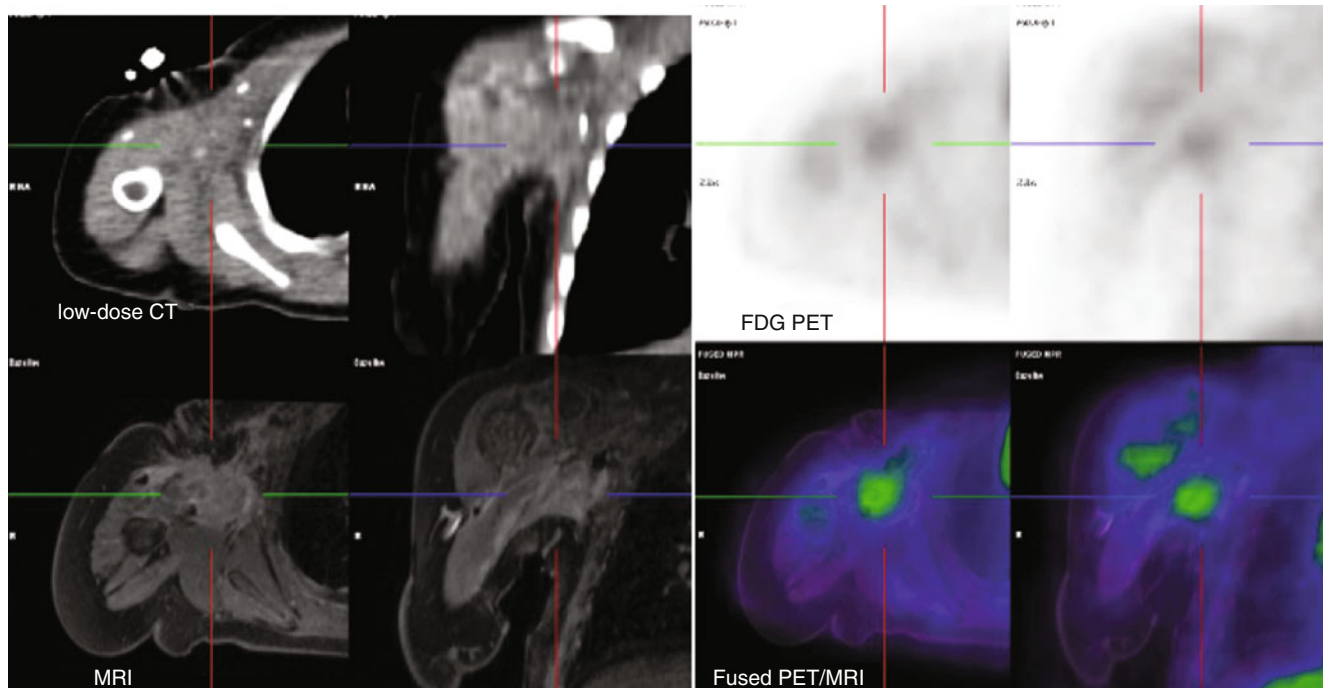


Fig. 2.6 Side-by-side comparison of CT, MR and PET images of a patient with previously irradiated fibrosarcoma. The tumour is poorly visualised on CT but the MRI shows a residual mass. The PET shows residual moderate FDG-avidity, and resection confirmed residual viable

tumour. Lack of soft tissue contrast, particularly lack of fat in children compromises anatomical evaluation on CT compared to MRI (Courtesy of Rod Hicks, Peter MacCallum Cancer Centre, Melbourne Australia)

musculoskeletal system. In addition to much improved soft tissue contrast MR is a versatile imaging modality since it provides additional measures of physiologic and metabolic characteristics of human tissue [25]. MRI goes beyond plain anatomical imaging by offering a multitude of endogenous contrasts and a high capability of differentiating soft tissues, as well as many exogenous contrast media ranging from gadolinium-based agents to highly specified cellular markers [26].

MR spectroscopy (MRS), for example, can be used to dissect the molecular composition of tissues by applying selective radiofrequency excitation pulses [27]. Functional processes in living subjects can also be studied via diffusion-weighted (DWI) MRI [28]. Here, a spatially and temporally variant magnetic field, generated by different magnetic field gradients in all three spatial directions, is used to map phase differences in the MRI signal that are caused by diffusing molecules. DWI-MRI has potential clinical applications ranging from diagnosing ischemia in early stroke diagnostics, cancer, multiple sclerosis, or Alzheimer's disease to general fiber tracking via diffusion tensor imaging (DTI) [26, 29, 30], and it is not restricted to the brain [31]. In addition, functional MRI (fMRI) studies can be performed during the same examination. Functional MRI (fMRI) studies are frequently based on the BOLD (blood oxygen level dependent) effect [32]. This effect describes the fact that the magnetic properties of oxygenated and deoxygenated hemoglobin in the blood are different and, therefore, produce

different signals when imaged with T2*-sensitive MRI sequences. The BOLD effect also has certain applications in cancer imaging, such as to study tumor angiogenesis, tumor oxygenation and brain activation in eloquent areas prior to surgical resection.

Any of the image information above can be acquired and presented in any direction in space, thus rendering re-orientation of image information in MR similar to a “virtual tilt”, that is available in CT-only in directions perpendicular to the main scanner axis, and that are not available in PET/CT imaging.

Similar to CT and PET, MRI has become a whole-body imaging modality thanks, for example, to the advent of parallel imaging techniques and all their derivatives [33–35] and thanks to new whole-body imaging strategies [36, 37]. Image acquisition times have been shortened, thus allowing fast single-contrast MR whole-body coverage from 30 s [36] ranging to multi-contrast, multi-station whole-body MRI examinations to be acquired with high spatial resolution in less than 1 h. Initial results show that whole-body MRI is a promising modality in oncology, especially for the detection of metastases and hematologic malignancies.

Therefore, MRI holds a great potential in replacing CT as the complementary modality to PET in dual-modality tomographs for selected indications where MR outperforms CT already. In theory, MRI seems a perfect anatomical complement to PET.

PET/MR Design Concepts

Following the successful adoption of PET/CT in clinical routine and the ongoing efforts towards combining PET and MRI for pre-clinical research applications [24], industry has quickly adopted the idea of combining PET and MRI for human studies. Figure 2.7 summarizes the main approaches towards PET/MR hardware fusion. In essence, three different design concepts have been proposed: separate PET/CT and MRI systems operated in adjacent rooms (a), PET and MRI systems arranged in the direction of the main scanner axis with a patient handling system mounted in between (b) and a fully integrated PET/MRI system (c).

PET/CT-MR Shuttle System

GE Healthcare proposed a straightforward design in late 2010. This design is based on a combination of a dual-modality, whole-body TOF-PET/CT and a 3 T MR system that are operated in adjacent rooms; patients are shuttled from one system to the other without getting off the bed [38]. This approach substitutes the challenges of hardware integration for immense logistical challenges in timing access to the two systems while minimizing patient motion in between examinations. The advantage of this rather simplistic approach to PET/MR is that it is based on existing imaging technologies without significant changes to their hardware components. Patients undergo a PET/CT study leveraging the benefits of time-of-flight PET as discussed before. Following the PET/CT examination patients are then lifted on a mobile docking-table system and shuttled to the MR system where a loco-regional or whole-body MR study is performed depending on the clinical indication. Figure 2.8 illustrates a clinical case from the combined use of PET/CT and MRI using the PET/CT/MR system.

While this design is still available as prototype technology only, it has been argued also as the most cost-effective compared to fully integrated PET/MR based on workflow aspects and machine utilization [39], both of which are site- and operations dependent. Therefore, in practice the clinical and cost efficacy of the separate PET/CT/MR design option (Fig. 2.7a) would be affected by various workflow and installation requirements. For example, both systems need to be installed next to each other and operated within a combined scheduling system. Any deviation from standard protocols would entail extended waiting times with the patients lying on the shuttle system until the next exam can commence. Also, two or even three shuttle systems are required to facilitate a seamless, high-throughput workflow. On the upside this approach does ensure proper attenuation and scatter correction of the PET data based on the available CT information. In

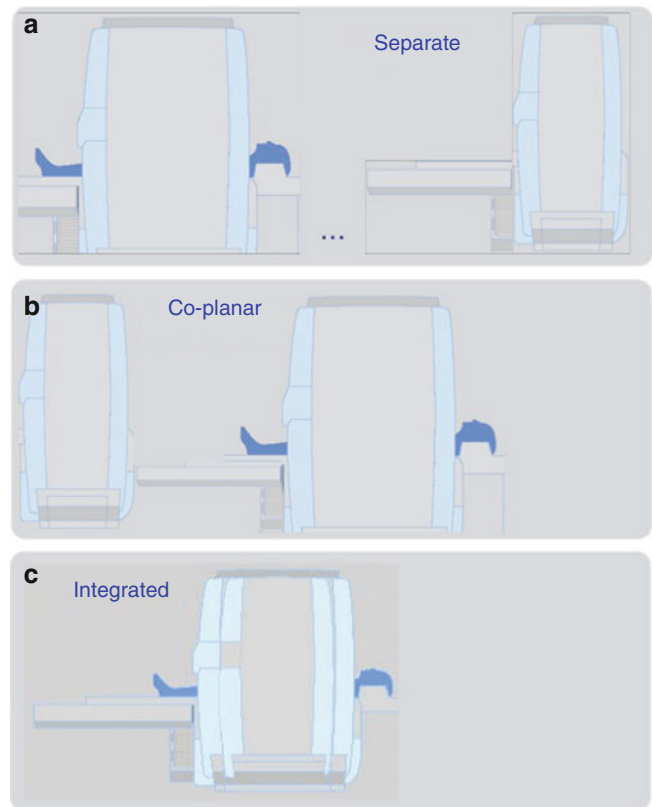


Fig. 2.7 Design concepts for PET/MR: PET/CT and MRI tomographs are operated in adjacent rooms and interlinked with a mobile shuttle system (a), a co-planar PET/MR with a whole-body PET and MR operated in close proximity and a combined table platform (b), and a fully integrated PET/MR with MR-compatible PET detection system slip-fit into the MR (c)

turn, the examination time is likely to be the longest of all PET/MR designs and patient convenience is limited by the repositioning in MR or PET/CT using the shuttle system.

Co-planar PET/MR

Philips Healthcare proposed a slightly more integrated approach to PET/MR in 2010 [40]. They also presented the first commercially available PET/MR system for clinical use called the Philips Ingenuity TF PET/MRI. The system (Fig. 2.7b) is based on a co-planar design concept that integrates a whole-body time-of-flight (TOF) PET system and an Achieva 3 T X-series MR system. Both components are joined by a rotating table platform mounted in between [41].

The PET detector and electronics system is based on available Philips PET/CT technology. However, given the proximity of the PET and MR system (about 4 m) some modifications were required to ensure MR-compatibility of the PET system. These modifications include the addition of bulk magnetic shielding of the PET to reduce fringe magnetic fields, the use of higher permeability shields of the photomultiplier tubes

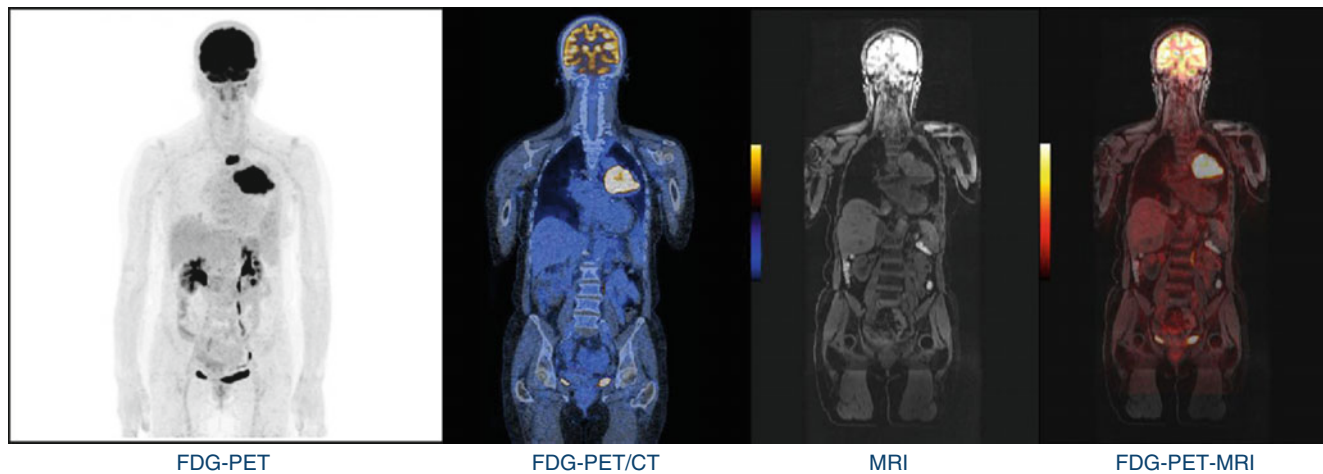


Fig. 2.8 Patient with large left lung lesion undergoing whole-body FDG-PET/CT and whole-body MRI on the separate PET/CT/MR system (Fig. 2.7a). From left to right: FDG-PET following CT-based attenuation correction (CT-AC), PET after CT-AC fused with whole-body

CT, complementary WB-MR and retrospectively aligned and fused PET/(CT)-MR (Data courtesy of Patrick Veit-Haibach, MD, University Hospital Zürich)

(PMT) inside the PET gantry and the rotation of the cathodes of the PMT's. Further, power and signal cables penetrating the room walls need to be filtered through specially designed radiofrequency (RF) penetration panels to prevent extraneous electromagnetic radiation to enter the scanner room and PET acquisition electronics are enclosed in an RF tight cabinet. These and other modifications are discussed in more detail in [41]. The authors show that despite the modifications to the PET/MRI system components the performance of neither the PET nor of the MR is degraded, and that both systems can be operated in close spatial proximity.

Figure 2.9 illustrates a total-body imaging examination from the co-planar PET/MR system. While this design concept may be regarded as a step closer towards integrated PET/MR (compared to sequential imaging, Fig. 2.7a) it offers sequential PET and MRI imaging with delays that are on the order of those in PET/CT and in sequential PET/CT-MR imaging [42]. It could be argued that co-registration of PET and MR information is slightly better and, perhaps more reproducible, in both modalities compared to the shuttle system in Fig. 2.7a, since patients are not relocated between rooms and repositioned using a mobile patient handling system. However, no study to date has been able to verify this. Unlike with the separate PET/CT-MR system, one modality is idling during co-planar PET/MR imaging, which may be argued to be less cost-effective. However, one should keep in mind that today few indications are clearly defined as key indications for PET/MR, and, therefore, throughput is likely not an issue for the time being. The co-planar PET/MR system offers full MR-flexibility and TOF-PET functionality. Unlike with the separate design, no transmission source is available, thus requiring MR-based attenuation correction methods (see below).

Integrated PET/MR

The first PET/MR design for human use was presented as early as in 2006, representing also the most challenging design concept (Fig. 2.7c) [43]. This PET/MR prototype system (BrainPET, Siemens Healthcare) was intended for brain imaging only and considered a proof-of-concept for a fully integrated PET/MR. The BrainPET system was based on a PET detector ring designed as an insert to a 3T whole-body MR scanner (Magentom Trio, Siemens Healthcare Sector, Erlangen, Germany) with the novelty being the MR-compatible PET detection system that was integrated into the MR system. Here, the PMT were replaced by Avalanche photodiodes (APD), which have been shown to operate in magnetic fields of up to 7 T [44] (see also section “MR-Compatible PET Detectors”). Therefore, in this design LSO (lutetium oxyorthosilicate)-based detector blocks, comprising of a 12×12 matrix of $2.5 \times 2.5 \times 20$ mm³ crystals were directly coupled to a compact 3×3 APD array. With this system PET and MRI cover an active co-axial FOV of 19.3 cm simultaneously. The point source sensitivity of the PET system measured with a line source in air was 5.6 % and the spatial resolution was 2.1 mm at the centre of the FOV. No degradation of the MR images was observed due to the presence of the PET detectors and no detrimental effect on the performance of the PET detectors was observed for a number of standard MR pulse sequences [45]. Since 2006 the BrainPET was installed at 4 sites worldwide, with one site operating the PET insert inside a 9.4 T MRI as well. Some preliminary clinical research data are described in [46–48]. Looked upon retrospectively, the clinical test phase of the BrainPET helped pave the road towards whole-body PET/MR, the advanced development of MR-based attenuation

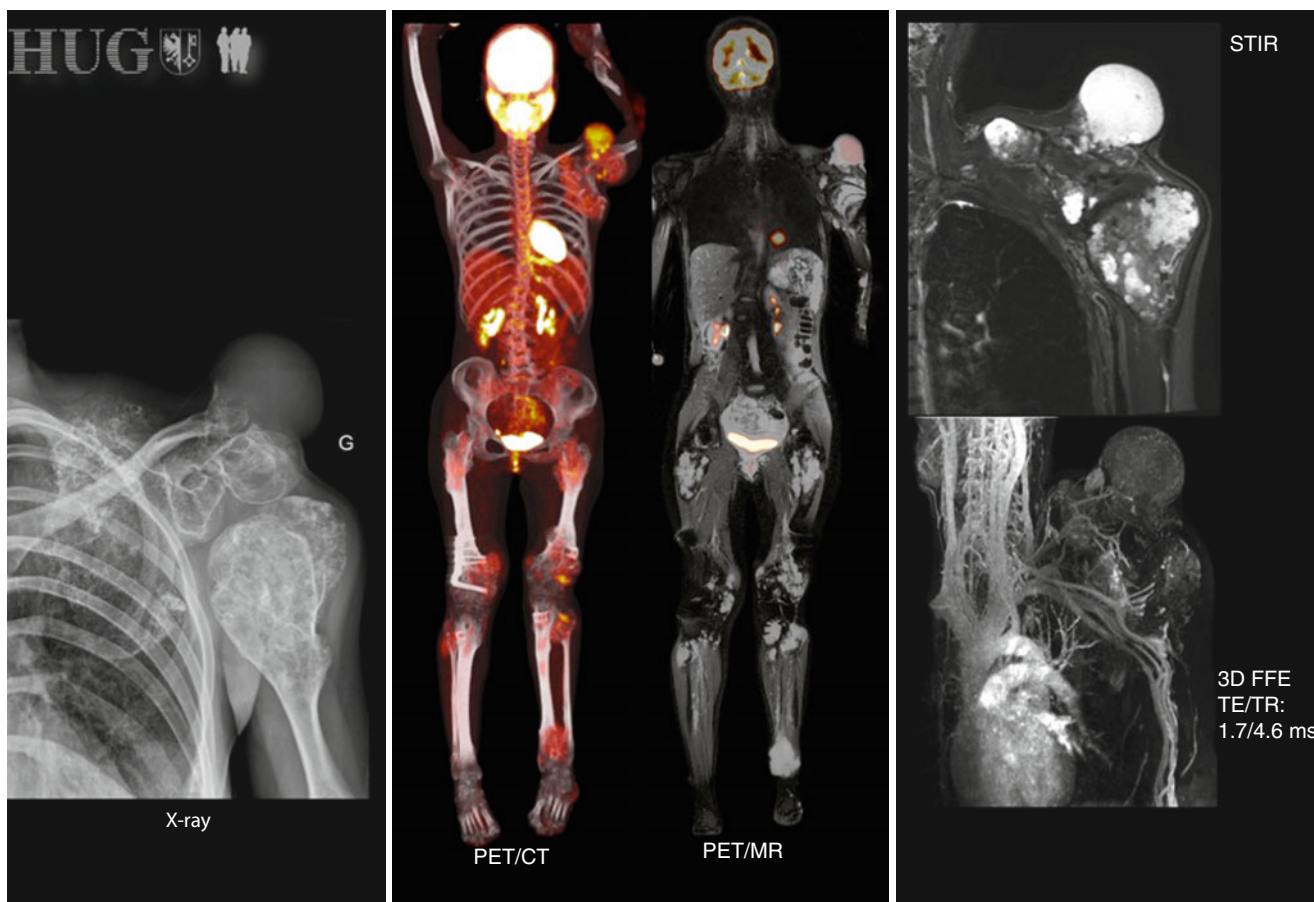


Fig. 2.9 29-y/o female patient with Maffucci syndrome diagnosed in her childhood. This disease is sporadic with multiple enchondromas and hemangiomas. An [18F]-FDG-PET/CT total body study was performed for staging. Subsequent total-body PET/MR, using the same

FDG injection, more clearly presents bone involvement and is preferred because of the need of multiple follow-up examinations (Data courtesy of Osman Ratib, MD, University Hospital Geneva)

correction and, perhaps most importantly, an improved communication and closer collaboration of radiologists, nuclear medicine physicians and physicists.

Based on the aforementioned positive BrainPET experiences a further step towards the integrated design concept (Fig. 2.7c) was suggested in late 2010. Then, the first whole-body, integrated PET/MRI system (Biograph mMR, Siemens Healthcare) was proposed. Each PET detector block consists of an 8×8 matrix of LSO crystals coupled to a 3×3 APD-array. The transaxial FOV of the MR is 50 cm, whereas the axial FOV is 45 cm. The PET subsystem consists of 8 rings of 56 blocks with an axial FOV of 25.8 cm and ring diameter of 65.6 cm. Both, the extended axial FOV of the PET and the reduced ring diameter help increase the sensitivity of the PET insert, which in turn could be leveraged, for example, for shorter emission scan times or reduced injected PET activities. Thus, the lack of TOF-capability in APD-based PET systems (see Chap. 3) can be compensated for, in theory, by bringing the PET detectors closer to the centre of the FOV and by extending the axial coverage. A detailed description of the system together with a performance characteristic

can be found in [49]. On the downside of the closer integration the integrated PET/MR system, the bore diameter is reduced to 60 cm, which – for the moment – is the reverse trend of PET/CT and MR-only instrumentation with gantry and bore diameters of up to 80 and 70 cm, respectively. Increased gantry and bore diameters help improve patient comfort and compliance and, in addition, leave room for image-guided interventions, if needed.

Perhaps most importantly, the integrated PET/MR design concept allows for simultaneous data acquisition. However, simultaneity of complementary volumetric data acquisition is assured only for a selected MR sequence and emission data that are acquired for the duration of that specific MR sequence. Nonetheless, simultaneous PET/MR is argued to improve the diagnostic accuracy of combined PET/MR over sequential imaging (Fig. 2.7a, b). Figure 2.10 illustrates a case from the Biograph mMR system with very good spatial alignment of PET and MR images in the abdomen.

While the benefit from improved spatio-temporal alignment is immanent to the PET/MR images from integrated PET/MR it is not clear as to how much it is required for clinical

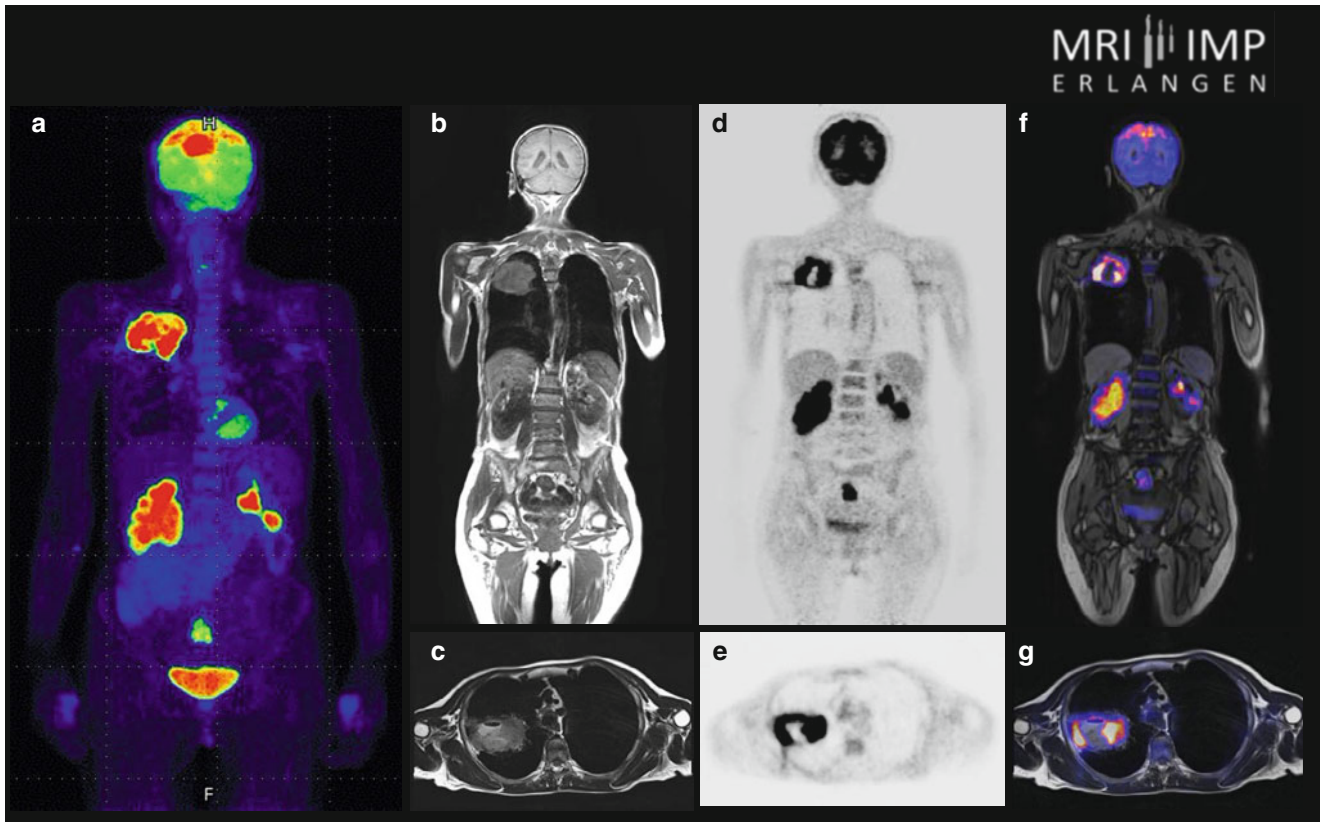


Fig. 2.10 61-y/o female with known squamous cell carcinoma of the lung undergoing [18F]-FDG-PET/MR imaging on an integrated Biograph mMR PET/MR system. (a) Increased PET tracer activity synonymous of disseminated disease is depicted in the bronchial carcinoma, frontal lobe metastasis, pancreas and in secondary, metastatic colorectal cancer. Coronal whole-body T1-weighted MR image (b),

attenuation corrected PET (d), and PET/MR image (f) and corresponding axial images through the bronchial carcinoma are shown (c, e, g)

routine. Further, PET and MR data are simultaneously acquired only for a limited period of time or for a selected region, or voxel in its extreme. Without a doubt, the closer alignment of PET and MR data in both, an anatomical framework and over various imaging times will help in clinical research, such as when comparing perfusion studies with [15O]-water and arterial spin labeling (ASL) in MR [24]. Also, using integrated PET/MR imaging for shortening combined examination times over those in sequential and co-planar designs is preferred for the well-being of patients with acute diseases, pediatric patients requiring sedation and patients with neurodegenerative diseases. Finally, since MR-based motion detection is conceivable during simultaneous PET/MR imaging, such MR-derived motion vector can potentially be used to correct for motion-induced blurring of the PET emission data [50, 51].


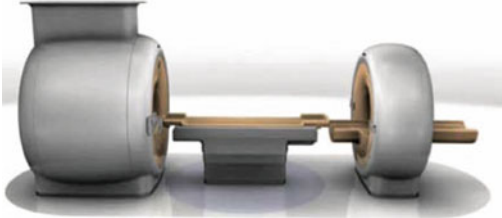

As with the co-planar design, the integrated PET/MR design does not allow for separate transmission imaging and, therefore, PET-based attenuation data must be derived from the available MR information. Thus, a normal workflow starts with the simultaneous acquisition of emission data and a dedicated MR sequence for the purpose of deriving attenuation data. As soon as the short MR-attenuation sequence is complete, additional diagnostic MR sequences can be

acquired for the remainder of the pre-defined emission scan. Alternatively, the PET emission data can be acquired in list-mode format and reframed after finishing the MR scan.

Table 2.2 provides an overview of currently available PET/MR systems. All systems support the acquisition of whole-body, if not total-body, examinations. These first PET/MR design concepts vary more widely than the first concepts for PET/CT. This variation can be explained by the complex physical and more demanding technical requirements for a full integration of PET and MR imaging systems, compared to those from a PET/CT integration.

The foremost difference between the PET/MR systems is the type of PET detector. Integrated PET/MR imaging requires a novel PET-based detection system, which will be explained in more detail in Chap. 3. APD-PET does not support TOF-based acquisitions due to the insufficient timing resolution of the APD, thus, only two PET/MR designs offer TOF-capabilities (Table 2.2). Major differences are also seen in the patient table design, which has subsequent effects on the handling of the patients and workflow. Both, the co-planar and the integrated PET/MR require the use of the MR images for human soft tissue attenuation correction, which today is perhaps the biggest challenge for combined PET/MR in the

Table 2.2 State-of-the-art PET/MR imaging systems by GE Healthcare, Philips Healthcare and Siemens Healthcare (from left to right). Note, as of 2012 the Philips and Siemens system were FDA-approved and commercially available. The figure shows key parameters and performance measures of the various PET/MR series

Discovery PET/CT-MR	Ingenuity TF	Biograph mMR
		
MR Discovery MR 750w 70 cm bore diameter 50 x 50 x 45 cm FOV 16 (32) receive channels 0.5 ppm field homogeneity	MR Achieva 3T TX 60 cm bore diameter 50 x 50 x 45 cm FOV 16 (32) receive channels 0.5 ppm field homogeneity	MR 3T (not Verio-based) 60 cm bore diameter 50 x 50 x 45 cm FOV 18 / 32 receive channels 0.1 ppm field homogeneity
PET Discovery PET/CT 690 4.2 x 6.3 x 25 mm ³ LYSO(Ce) 81 cm detector ring diameter Time-of-flight PET 15.7 cm axial coverage 70 cm bore diameter	PET 4.0 x 4.0 x 22 mm ³ LYSO(Ce) 90 cm detector ring diameter Time-of-flight PET 18 cm axial coverage 70 cm bore diameter	PET 4.0 x 4.0 x 20 mm ³ LSO 66 cm ring diameter No Time-of-flight option 25.8 cm axial coverage 60 cm bore diameter
Patient handling system Shuttle and docking system 159 kg patient load 170 cm co-scan range CT-based AC	Patient handling system Turning table platform 200 kg patient load 190 cm co-scan range MR-based AC	Patient handling system Integrated table platform 200 kg patient load 140 cm co-scan range MR-based AC
In-plane resolution: 4.9 mm Axial resolution: 5.6 mm 3D Sensitivity: 7.0 cps/kBq Peak NECR: 130 kcps Coincidence : 4.9 ns TOF resolution: 549 ps	In-plane resolution: 4.9 mm Axial resolution: 4.9 mm 3D Sensitivity: 6.4 cps/kBq (NEMA) Peak NECR: >91kcps @ 16kBq/ml Coincidence : 3.8 ns TOF resolution: 535 ps	In-plane resolution: 4.5 mm Axial resolution: 4.5 mm 3D Sensitivity: 13.2 cps/kBq Peak NECR: 175 kcps Coincidence : 5.9 ns No TOF

light of clinically adopted PET/CT imaging when absolute quantification of PET data is considered.

MR-Compatible PET Detectors

Cross-talk effects between PET and MRI may occur when inserting a conventional PET detector and associated electronic components into an existing MR system. This may relate to disruptions of the PET signal cascade as well as to degraded MR imaging. The possible interactions between PET and MR signal generation are manifold. A perfect technical integration of both modalities requires the MR with its electromagnetic environment not to disturb the sensitive PET signals. This encompasses the strong static and homogeneous magnetic field for spin alignment (in the range of several Tesla), the strong spatially (mT/m) and temporally (mT/m/ms) varying electromagnetic gradient fields for

spatial signal localization, as well as the pulsed radiofrequency (RF) transmit and receive fields for spin excitation and RF signal reception (MHz range). On the other hand, PET system components must not interfere with any of the above listed electromagnetic fields of the MR system.

Consequently, for a fully-integrated PET/MR system, all PET electronics must be RF shielded in order not to disturb the highly sensitive RF signals detected by the MR components. When shielding the PET components that are located close to the MR gradient coils, the RF shielding has to be designed such that the strong time variant gradient pulses do not produce unwanted Eddy currents in the shielding, which may have a negative effect on the gradient linearity, potentially leading to image distortions [52].

Given the design of standard PET detectors based on photomultiplier tubes (PMTs), a PET/MR configuration is obviously technically more challenging than the combination of PET and CT because phototubes are sensitive even to low

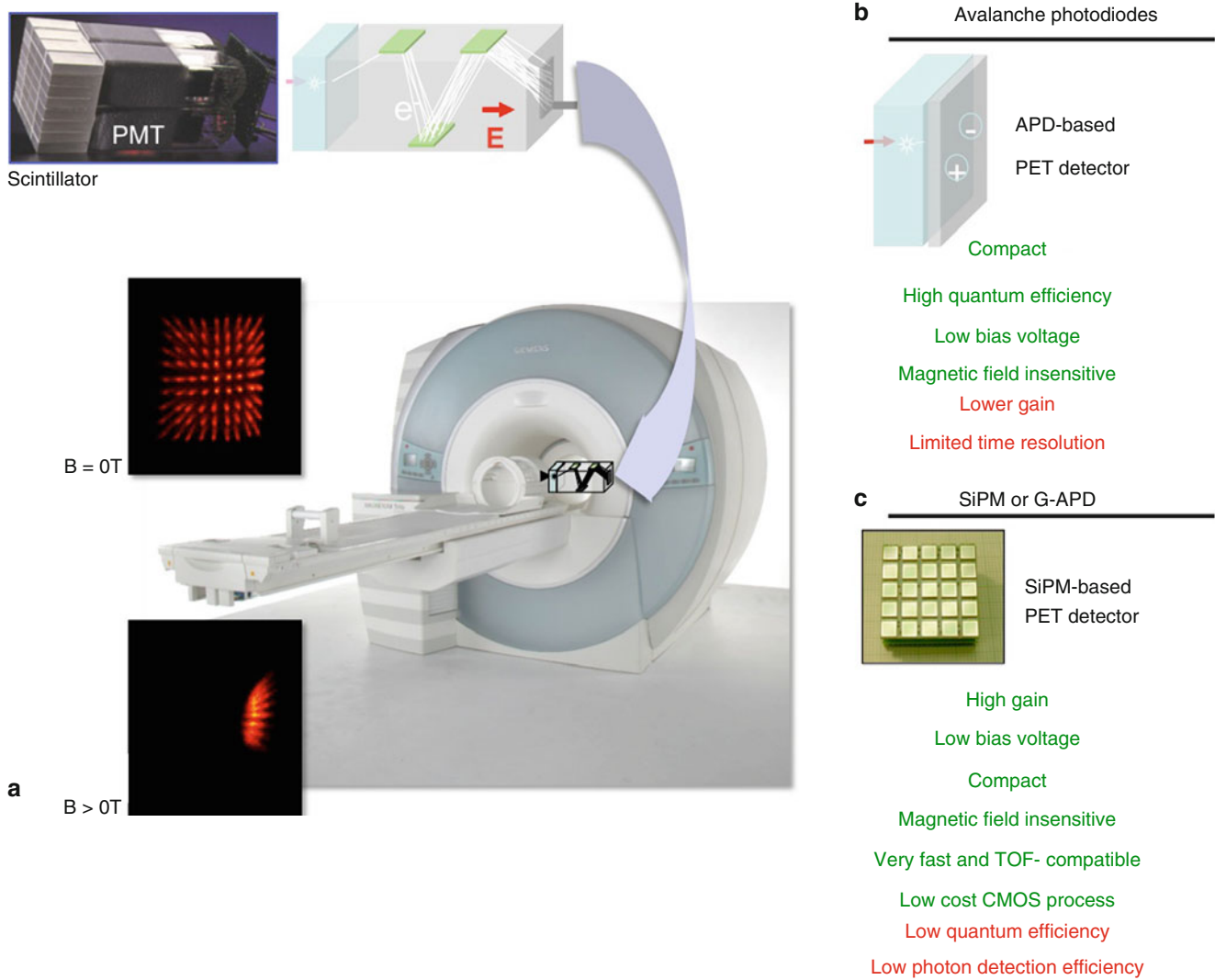


Fig. 2.11 (a) Conventional PET detectors using photomultiplier tubes (PMT) do not work inside a magnetic field. This is illustrated by the scintillator position profile that is skewed already from fringe fields from a horseshoe magnet placed next to the PET detector/PMR (Courtesy Bernd Pichler, University of Tübingen). New PET detectors

(b) based on avalanche photodiodes (APD) can be made more compact and have been shown to perform in magnetic fields up to 9.4T. Recent developments indicate further improvements for MR-compatible PET detectors based on SiPM, a type of Geiger-APDs (c)

magnetic fields (Fig. 2.11). Therefore, early developers of PET/MR concepts, such as Hammer and co-workers, proposed to place only the PET scintillator inside the MR and to use light guides to channel the scintillation light from the detector to the PMT situated outside the primary magnetic field of the MR system [53]. This idea was advanced further by other groups, as discussed by Wehrl in a recent review of the origins of PET/MR [24].

In order to provide PET performance in PET/MR that is similar to PET performance in PET/CT, any MR-compatible PET detector must support accurate 3D positioning and very fast timing information at no cost of volume sensitivity. This, in turn, calls for combinations of scintillators with novel, MR-compatible photodetectors of high granularity such as Avalanche Photodiodes (APD) and Silicon Photomultipliers (SiPM) [54].

Avalanche Photodiodes (APD)

Avalanche photodiodes (APD) are semiconductor devices that transform detected light into an electrical signal following the same principles as ordinary photodiodes. However, unlike ordinary photodiodes, APD's operate exclusively at high electric fields. When an electron–hole pair is generated by photon absorption, the electron (or the hole) accelerate and gain sufficient energy from the high electric field before it collides with the crystal lattice and generates another electron–hole pair while losing some of its kinetic energy in the process (Fig. 2.11b). This process is known as impact ionization. The original as well as the secondary electron (or hole) can then accelerate again under the influence of the high electric field and create more electron hole pairs. This process creates an avalanche of electron hole pairs – hence

the name avalanche photodiodes. The rate at which electron–hole pairs are generated by impact ionization is balanced by the rate at which they exit the high-field region and are collected. If the magnitude of the electric field (reverse-bias voltage) is below a value known as the breakdown voltage, the rate of collection exceeds that of electron hole creation and causes the population of electrons and holes to decline and eventually stops.

The number of created electron–hole pairs, referred to as internal gain, is typically in the range of 10^1 – 10^3 and dependent on the electric field strength (reverse bias voltage). Because the average number of created electron–hole pair is strictly proportional to the incident light photons, this mode of operation is known as linear mode.

Unlike amplification in PMTs, the internal gain of APDs is characterized by fluctuations due to the statistical nature of impact ionization. These gain fluctuations produce excess noise, which increases as the internal gain increases by raising the reverse bias. Other factors that affect the performance of APD include temperature, doping, as well as diode material properties. In addition, APDs are characterized by a relatively long timing resolution ($\text{FWHM} > 1,000$ ps), which limits their use in TOF PET systems. Because of these factors, it is desirable to use APDs at moderate reverse bias voltage and temperature to ensure their stable operation.

On the other hand, APDs are characterized by high quantum efficiency (QE – number of electron or holes created per number of incident scintillation photons) particularly at the wavelengths of PET scintillation detectors. APDs are also immune to after-pulsing, which are spurious pulses generated from electron-holes being trapped by crystal defects and released after a certain delay time, thus, confounding the detection process. Most importantly and contrary to PMTs, APDs are immune to stationary and varying magnetic fields, thus, rendering them suitable for PET/MR systems. APDs typically have a maximum size limited to about 1 cm^2 , due to the difficulty of manufacturing large area semiconductor devices, however, the cost of manufacturing APDs is relatively low.

Silicone Photomultipliers (SiPM)

A promising development in photodetection for PET imaging is the introduction of Geiger mode avalanche photodiodes (G-APD, Fig. 2.11c), commonly referred to as silicon photomultiplier (SiPM). This is a novel type of photodetector that is about to reach a performance level that offers significant improvement over APD-based PET.

A SiPM is an APD operated with a reverse bias voltage above the breakdown voltage (~ 50 – 60 V above breakdown voltage). In this case, the electron hole pairs generated by photon absorption will multiply by impact ionization faster than they can be extracted, thus, resulting in an exponential

growth of electron–hole pairs and their associated photocurrent. This process is known as Geiger discharge. The current flow produced by the Geiger discharge is large and results in a large signal gain (more than 10^5). Following a Geiger discharge, the SiPM is reset by dropping (quenching) the voltage across the photodiode below the breakdown voltage. This will reduce the number of created electron hole pairs and eventually stop the Geiger discharge. The discharge-and-reset cycle is known as the Geiger mode of operation of the photodiode. The turn-on transient of the current discharge is comparatively fast, with several picoseconds while the turn-off transient through quenching is mostly dependent on the SiPM size and is on the order of 100 ns. Quenching can be achieved using active or passive techniques although for high counting capabilities, active quenching is preferred.

One important application of SiPMs is their ability to count photons, which could be used to determine the energy of the incident annihilation photon on a scintillator in a PET system. However, a single SiPM cell has a limitation in that it is essentially either on or off. It cannot distinguish between a single and multiple photons that arrive simultaneously. One only knows that the APD was triggered. This limitation, however, is overcome when using an array of SiPM cells that are connected in parallel. In this case the output of the SiPM array is the sum of the output of each SiPM cell (pixel) in the array. For example, when the photon flux is low and photons arrive at a time interval longer than the recovery time of a pixel, the array will output pulses that equate to a single photoelectron. The generated pulses are then converted to digital pulses and counted. However, when the photon flux is high or the photons arrive in short pulses (pulse width less than the recovery time of the SiPM), the pixel outputs will add up to the equivalent number of incident photons. In this case, the SiPM array behaves in a pseudo-analog manner, because it can measure the incident number of photons per pulse, which is not possible with single photon counting SiPMs.

An important feature of SiPMs is their immunity to excess noise. This is primarily due to the fixed number of electron–hole pairs produced in Geiger mode, which is not defined by the statistics of the impact ionization process as in APDs. Another important feature of SiPMs is their relatively fast rise time, and short time jitter ($\text{FWHM} = 0.1$ ns) defined as the statistical variation of time interval between the photon arrival and the resulting electrical signal from the SiPM – thus, supporting their use in TOF-PET tomographs. Furthermore, the performance of SiPMs (like APDs) is immune to the effects of stationary and temporally varying magnetic fields which allows their use in PET/MR systems.

On the other hand, SiPMs have a relatively low photon detection efficiency (PDE), due to their low QE for scintillation light from PET detectors (40 % at 420 nm). In addition, SiPMs are characterized by high dark count rate, high cross talk and after pulsing as well as a strong temperature and

Table 2.3 Characteristics of photodetectors for PET

	PMT	APD	SiPM
Active area (mm ²)	1–2,000 cm ²	1–100 mm ²	1–10 mm ²
Gain	10 ⁵ –10 ⁷	10 ²	10 ⁵ –10 ⁷
Rise time	<1 ns	2–3 ns	~1
Dark current/countrate	<0.1 nA/cm ²	1–10 nA/mm ²	0.1–1 MHz/mm ²
Capacitance (pF/mm ²)	9	2–10	>30
QE @ 420 nm (%)	25	60–80	<40*
Afterpulsing	Yes	No	Yes
Bias voltage (V)	1,000–2,000	~200–1,500	~50
Power consumption	100 mW/ch	10 μW/mm ²	<50 μW/mm ²
Temperature coefficient	<1 %/°C	2–3 %/°C	3–5 %/°C
Bias coefficient	<1 %/V	10 %/V	~100 %/V
Magnetic susceptibility	Very high (mT)	No (up to 9.4 T)	No (up to 15 T)

Information adapted from [54]

*Photon detection efficiency rather than quantum efficiency (QE)

timing dependence on bias, all of which reduce the performance of SiPMs. Table 2.3 shows a comparison between the performance characteristics of APDs, SiPMs, and PMTs.

Recent developments focusing on SiPM intend to create a fully-digital data handling of PET detector signals without employing dedicated read-out, amplifier ASICs, ADCs, etc. Such a fully-digital SiPM (dSiPM) was first presented in 2009 by Frach, Degenhardt and colleagues from Philips Research Aachen [55]. The dSiPM contains over 8,000 G-APDs on a 4 × 3 mm layer. In a laboratory set-up the coincidence timing resolution using a ²²Na source and 3 × 3 × 5 mm³ LYSO crystal coupled to dSiPM was 153 ps FWHM and the energy resolution at 511 keV was 10.7 % FWHM. Further advances are expected towards integrating these detection systems in clinical systems, which would certainly be of great benefit for PET/MR systems.

PET/MR Methodological Pitfalls and Technological Challenges

MR-Based Attenuation Correction

In addition to the technical challenges of combining PET and MRI the necessary attenuation correction factors for the PET emission data must be derived from the PET/MR measurements [56]. While in PET/CT PET attenuation data can be derived from transforming available CT transmission images into maps of attenuation coefficients at 511 keV [10], no such transmission data are available in PET/MR. This is primarily due to the lack of physical space to host a transmission source. Secondly, a rotating, metal-encased transmission source, whether X-ray tube, rod or point sources would lead to severe crosstalk with the MR magnetic field. And finally, the available MR images represent, in essence, proton densities that cannot be directly translated into maps of electron

densities as obtained from CT transmission measurements. For example, air and cortical bone yield no significantly measurable MR signal, whereas the difference in their photon attenuation properties is 2,500 HU on CT images (Fig. 2.12). Therefore, PET/MR requires novel approaches to MR-based attenuation correction (MR-AC).

Originally, straightforward segmentation-based approaches have been proposed to classify tissues on MR images and to assign respective attenuation coefficients. This approach seems to work well in brain imaging [57]. However, MR-AC in extra-cerebral applications is much more demanding [58]. Therefore, atlas-based approaches have been suggested for MR-AC of brain [59] and torso data [60].

The principle of the atlas approach is to align the MR acquired for the PET/MR study with an average MR image from an atlas comprising pairs of co-registered MR and CT data sets. The same transformation determined from the alignment of the MR of the patient with the MR in the atlas can be applied to the CT volume from the atlas. A combination of the co-registered CT image volume and the patient-specific MR can be used to generate a pseudo CT map of the PET/MR study from which the ACFs can be derived. In view of the absence of an MR bone signal, the bone structures can be extracted from the co-registered atlas CT and combined with an MR image segmented for air and soft tissue. Atlas-based approaches with or without pattern recognition enhancement do account for the presence of bone, but these algorithms are computationally demanding and require a set of aligned CT and MR image volumes for a given PET/MR system [60].

The current implementations of MR-AC of patient tissues are based on a combination of 3D Dixon-VIBE sequences in conjunction with subsequent image segmentation. Here, the gray values provided by the Dixon VIBE sequence are registered to different tissue classes resulting in tissue segmentation. The Dixon technique provides two images with water and fat being ‘in phase’ and in ‘opposed phase’. This allows

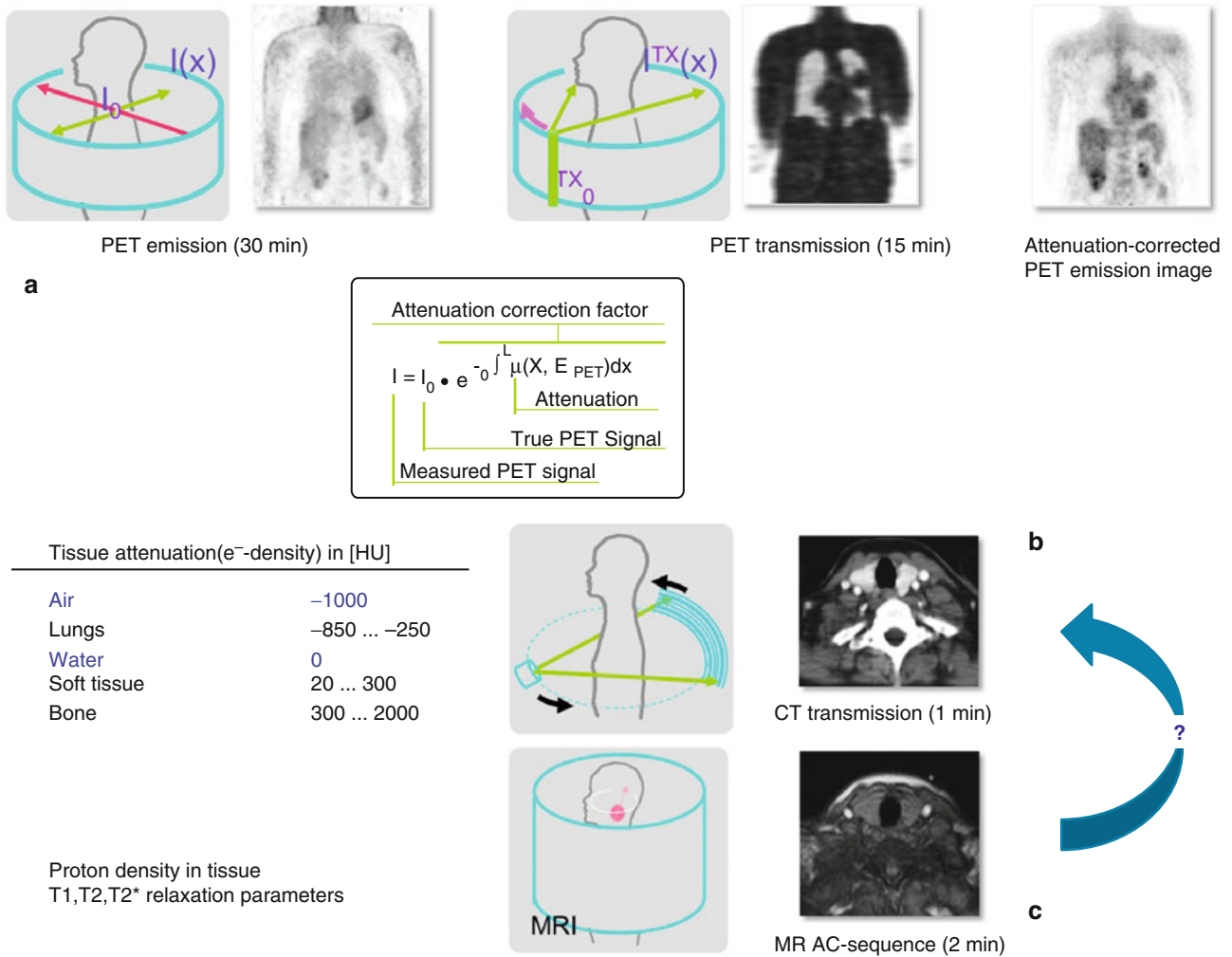


Fig. 2.12 Challenges of MR-based attenuation correction. (a) In PET attenuation correction factors can be calculated from separate PET transmission measurements, which take a relatively long time but provide attenuation values at 511 keV. (b) In PET/CT CT-based attenuation values, representing a measure of the electron-density, can be used to

estimate PET attenuation coefficients. (c) In PET/MR no measure of electron density is available and tissue appearance on MR and CT images is markedly different for air and bone. Therefore, no direct measurement is available for MR-based attenuation coefficients

for reconstruction of fat-only, water-only and fat-water images, and results in tissue segmentation of air, fat, muscle, and lungs [61]. Bone is not accounted for in this approach. Initial results in clinical pilot studies have shown that this approach works reliably and provides results that are comparable to corrected images from PET/CT in the same individual. However, further studies are needed to assess the impact of ignoring bone and the overall accuracy of MR-based AC methods on PET quantification.

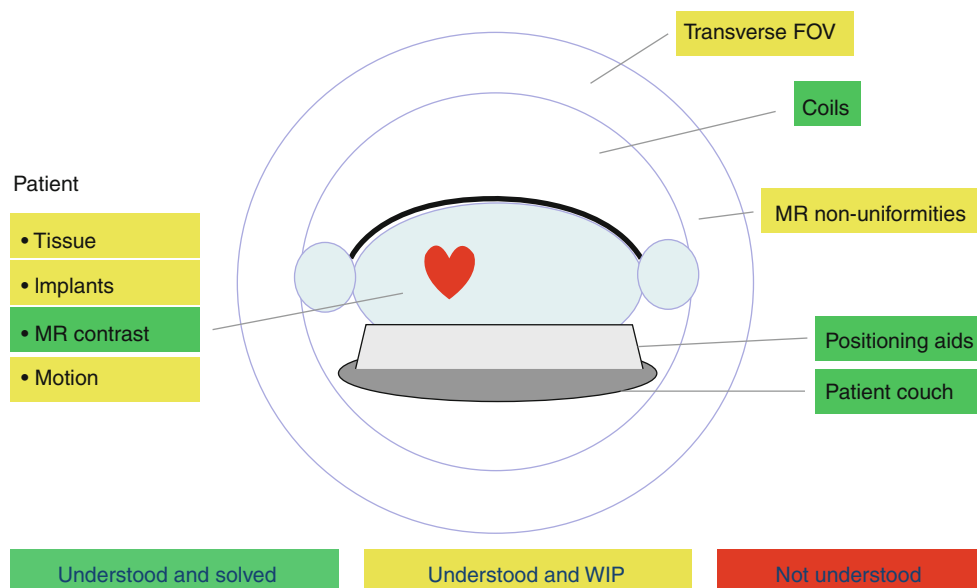
The Effect of MR Radiofrequency (RF) Coils on MR-AC

In addition to the general transformation of suitable MR image information of patient tissues, other, hardware-related attenuators must be considered during the transformation.

This relates to the patient table, transmit and receive radio-frequency (RF) coils as well as positioning aids. The fact that the RF coils are located inside the FOV of the PET system (Fig. 2.7b, c) is a challenge and has only started to be addressed. For brain scans, the head coil is rigid and its attenuation values can be estimated from a reference CT-based attenuation map. Subsequently for any PET/MR study only the relative position of the head coil inside the PET/MR system would be required. Additional work has been directed towards reducing the amount of attenuating materials in MR coils used in PET/CT as exemplified in a modified brain coil for integrated PET/MR imaging [62, 63].

For extra-cranial examinations the situation is more demanding. MR surface coils are required to achieve optimal signal-to-noise-ratio (SNR) and high quality MR images. Surface RF coils may contain elastic components and hence their individual position on the patient cannot easily be

Fig. 2.13 Contributors to attenuation and image distortions in PET/MR. Topics marked as *green* are resolved and addressed, those marked in *yellow* are known but solutions are work-in-progress



predicted. The effect of flexible body coils on overall PET attenuation was recently estimated by Tellmann and colleagues [64]. The authors report a maximum bias of 4 % in attenuation-corrected torso PET if surface coils are not accounted for during AC. This bias is negligible compared to the respective bias in head studies when ignoring dedicated, rigid head RF coils (up to 20 %). MacDonald and colleagues report similar results [65].

All PET/MR vendors today offer CT-based attenuation templates for rigid coils as well as for the patient bed that are seamlessly integrated during the attenuation correction. Nonetheless, clinical studies are required to further study the effect of misaligned RF coil templates and missing templates for accurate representation of flexible coils on PET quantification.

The Presence of MR Contrast Agents

MR-based AC could potentially be biased from the presence of MR contrast materials, which are typically made up of iron oxide and Gd-chelates for oral and intravenous (IV) application, respectively. It is known from the development of CT-based AC that the presence of contrast materials with atomic numbers higher than those of water may lead to biased attenuation maps for PET emission data. The same effects may occur with MRCA that are applied during PET/MR imaging. Furthermore, the presence of MR contrast agents may produce changes in the MR signal intensity that yield biased attenuation maps. First studies indicate no negative effect from MR contrast on PET quantification following MR-based attenuation correction [66, 67].

Limited FOV and Truncation Effects

Given the reduced bore diameter and the relatively long examination times in PET/MR compared to clinical PET/CT, most patients are positioned in the more comfortable position with their arms down. Thus, the patient anatomy may well extend beyond the transverse FOV of the MR (typically 50 cm), whereby the arms or the trunk of the patient are not fully covered by the MR images used for MR-AC. This may yield an underestimation of the reconstructed, attenuation-corrected emission activity concentration. Truncation artifacts were described for PET/CT imaging [68] and have been reviewed for PET/MR [69]. It was shown that with the arms extending beyond the FOV of the MR the PET activity following MR-AC was biased by up to 14 % in the area of truncation. The underestimated activity concentration could be recovered to within 2 % of the nominal concentration following simple, manual extension of the attenuation map.

An alternative solution would be to use the uncorrected PET image to estimate the patient cross-section in those areas outside the measured FOV where no – or only geometrically distorted – MR information is available [70, 71]. The clinical feasibility of this approach still needs to be validated. Particularly, in imaging scenarios with highly specific tracers the arms may be difficult to segment automatically in the uncorrected PET images.

Figure 2.13 summarizes the challenges and the status of MR-based attenuation corrections in PET/MR. Most challenges are understood with some being addressed sufficiently and some awaiting further optimization, validation and clinical adoption.

MR-Based Partial Volume Correction

As early as 1991, Leahy et al. suggested that PET reconstruction could be improved by using anatomical MR images from the same patient as prior information [72]. It is common clinical practice today for neurology patients with a PET-indication to also undergo an MR examination. However, MR-guided PET reconstruction has not yet made the transition from research into clinical routine. Aside from logistical problems associated with the retrieval of the complementary image sets, sub-optimal retrospective image alignment would significantly deteriorate the quality of the PET data [73]. However, in combined PET/MR imaging systems, the spatial (and temporal) alignment accuracy could be improved, thus, helping to promote the concept of MR-guided PET image reconstruction.

Even if the PET image is reconstructed independently of the MR image, it is still possible to use the MR image of the patient as an aid for improved quantification. In particular MR-guided partial volume correction (PVC) was suggested as early as in 1990 [74, 75]. Again PET and MR images from combined PET/MR examinations may facilitate improvements in MR-based PET quantification through the use of MR-based PVC.

MR-Based Motion Correction

Patient motion, from involuntary movements, and cardiac as well as respiratory cycles, is a major contribution to degraded PET image quality. In addition, patient motion will lead to local or extended mis-alignment of complementary anatomometabolic image information. In PET/CT, for example, the PET image is acquired over several minutes, while the CT scan is a matter of seconds and frequently acquired during a single breath hold. As a result, patient motion typically causes local misalignment between the PET and CT images and may lead to serious artifacts for AC, for example near the diaphragm. Dedicated breathing instructions have been shown to help reduce misalignment in the thorax and upper abdomen [76, 77]. Other authors have recommended 4D PET/CT acquisition and AC, however, this involves a substantially higher patient radiation dose [78–80].

Respiration is expected to generate misalignment and blurring in PET/MR images, too. As MR scans generally take much longer than CT scans, patients spend an even longer time in the PET/MR compared to PET/CT, and consequently patient motion is likely to cause even more severe artifacts. However, integrated PET/MR system technology offers a promising solution to the problem (Fig. 2.14). Various MRI motion-tracking techniques are available in clinical settings, including but not limited to cloverleaf navigators [81]. Such techniques have been tested with the BrainPET system with promising results from estimating

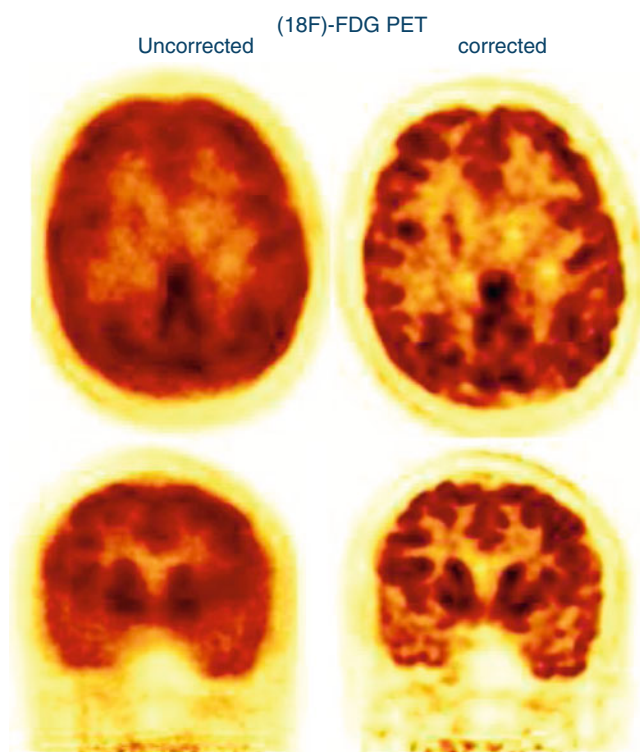


Fig. 2.14 FDG-PET images following attenuation correction (*left*) and motion+attenuation correction (*right*) clearly demonstrate the potentially improved quality of the data from lengthy examinations (Courtesy of J Scheins and H Herzog, Research Centre Jülich)

and correcting involuntary head motion as a result of relaxation of neck muscles. Using 3D Hoffman brain phantom and human volunteer studies, Catana et al. reported that high-temporal-resolution MRI-derived motion estimates acquired simultaneously on the hybrid BrainPET system (Siemens Healthcare) can be used to improve PET image quality, thus increasing its reliability, reproducibility, and quantitative accuracy [50].

Likewise, novel 3D cine sequences are under development to track spatio-temporal deformation of organs such as the heart and the thorax. Subsequently, deformation fields are generated and incorporated into the PET reconstruction [51, 82–85].

Thus, the use of periodic MR navigator signals in conjunction with a 4D model of the human torso may help to correct for motion-induced image degeneration in PET/MR data following 4D-MR-AC, which would be a major advantage over CT-AC.

PET/MR Safety

Combined PET/CT has been clinically very successful and may well serve as a benchmark for the development of PET/MR. However, despite the success of PET/CT there are also

shortcomings in the use of CT as the anatomical complement to PET. As such, CT uses a source of ionizing radiation for imaging and, therefore, adds significant radiation dose to the overall examination. Brix et al. have shown that the diagnostic CT contributes up to 75 % of the effective dose in patients undergoing whole-body FDG-PET/CT examinations for oncology indications leading to a total of about 25 mSv effective dose [86]. These dose levels may raise concern in selected population like adolescents and females. Figure 2.15a illustrates the relative contribution to patient exposure from the individual steps in a combined PET/CT examination.

In PET/MR examinations, overall patient exposure is reduced significantly by replacing the CT imaging step with an MR imaging sequence (Fig. 2.15b). In addition, MR provides advanced functional imaging information, such as DWI or MRS, without adding to the overall radiation exposure burden. Nonetheless, staff exposure is expected to increase slightly in PET/MR, given the complexity of the patient set-up when employing a range of surface RF body coils. However, no valid data are available as of yet.

Long-term experience and hundreds of millions of routinely and safely performed MR examinations confirm that MRI is a safe imaging modality. Nevertheless, a number of safety concerns do apply to PET/MR as discussed by Brix et al. [87], of which all are associated with the general safety issues known from MR-only imaging. The strong static magnetic field associated with MR systems potentially can attract ferromagnetic equipment as well as some patient implants, and accelerate these towards the strongest magnetic field in the isocentre of the PET/MR system. In some patients the strong and fast switching gradient fields may lead to peripheral nerve stimulation that are harmless but nevertheless disturbing. Finally, the strong-pulsed RF fields for MR signal excitation can cause tissue heating. As with all other RF transmitting devices, the RF power in MR imaging is limited to harmless values of the specific absorption rate (SAR) not leading to critical tissue heating. Some electric conducting metal implants, however, potentially may increase the local SAR values during an MR examination above the allowed SAR limits. To reduce all associated potential risks of MR imaging, patient questionnaires and patient screening and selection procedures have to be established and used in daily routine.

Accordingly, MR and PET/MR examinations of patients with passive implants (e.g., vascular clips and clamps, intra-vascular stents and filters, vascular access ports and catheters, heart valve prostheses, orthopedic prostheses, sheets and screws, intrauterine contraceptive devices), active implants (e.g., cardiac pace-makers and defibrillators, cochlear implants, electronic drug infusion pumps) or other objects of ferromagnetic or unknown material (pellets, bullets) are always associated with a potential risk. Careful pre-examination interviews of the patients regarding the presence or

absence of passive implants, which may interfere with the MR imaging protocol, or deter the patient from this examination all together is mandatory [87].

Summary and Conclusion

Multi-modality imaging instrumentation has evolved dramatically during the past decade. Combined SPECT/CT, PET/CT and, lately, PET/MR have revolutionized imaging and medical diagnosis. In these times of limited resources in healthcare and rapidly increasing radiation awareness, any predictions for future developments of PET/MR technology must take into account a variety of aspects, ranging from cost-effectiveness to overall radiation dose. While technological innovation, such as PET/MR, always pairs with enthusiasm and public interest, subsequent commercial systems must be affordable and strategies for their clinical implementation must be assessed for their health benefit to justify their pursuit within a local or global healthcare system [88]. The impressive advances in imaging technology of the past decade came at a cost, but at what point do these advances become cost-effective? Whole-body PET examinations that took 1 h at the start of the last decade now take 5 min on PET/CT; the actual imaging takes only a fraction of the time needed for patient preparation and positioning or reporting the study. Does the increased wealth of available information from the MR make up for the increased examination time?

The radiation dose to the patient incurred by PET/CT is clearly an issue. Although the ALARA (as low as reasonably achievable) principle is sound advice, there are clearly groups of cancer-sufferers such as those in children and young adults where the probability of inducing a second, radiation-associated cancer exceeds the benefits that can be accrued from the study. Different imaging strategies should then be adopted, such as MRI, optical imaging or ultrasound.

The commendable drive to reduce radiation exposure to patients has fostered an interest in a combination of PET with MRI. However, it is fair to assume that as long as diseases such as cancer and dementia remain primarily diseases of the elderly, the benefits of nuclear and X-ray imaging will largely outweigh the risks.

Will the coming decade witness the replacement of PET/CT by PET/MRI? Some believe it will, just as in the 1980s there were those who predicted that MRI would replace CT within 5 years. Of course that never happened, as both techniques have strengths and weaknesses and they have each found their niche in the medical imaging armamentarium. The same is likely true of PET/CT and PET/MRI—the technical challenges will be solved and simultaneous acquisition of MRI and PET will undoubtedly open new doors in clinical research and eventually also in the clinic.

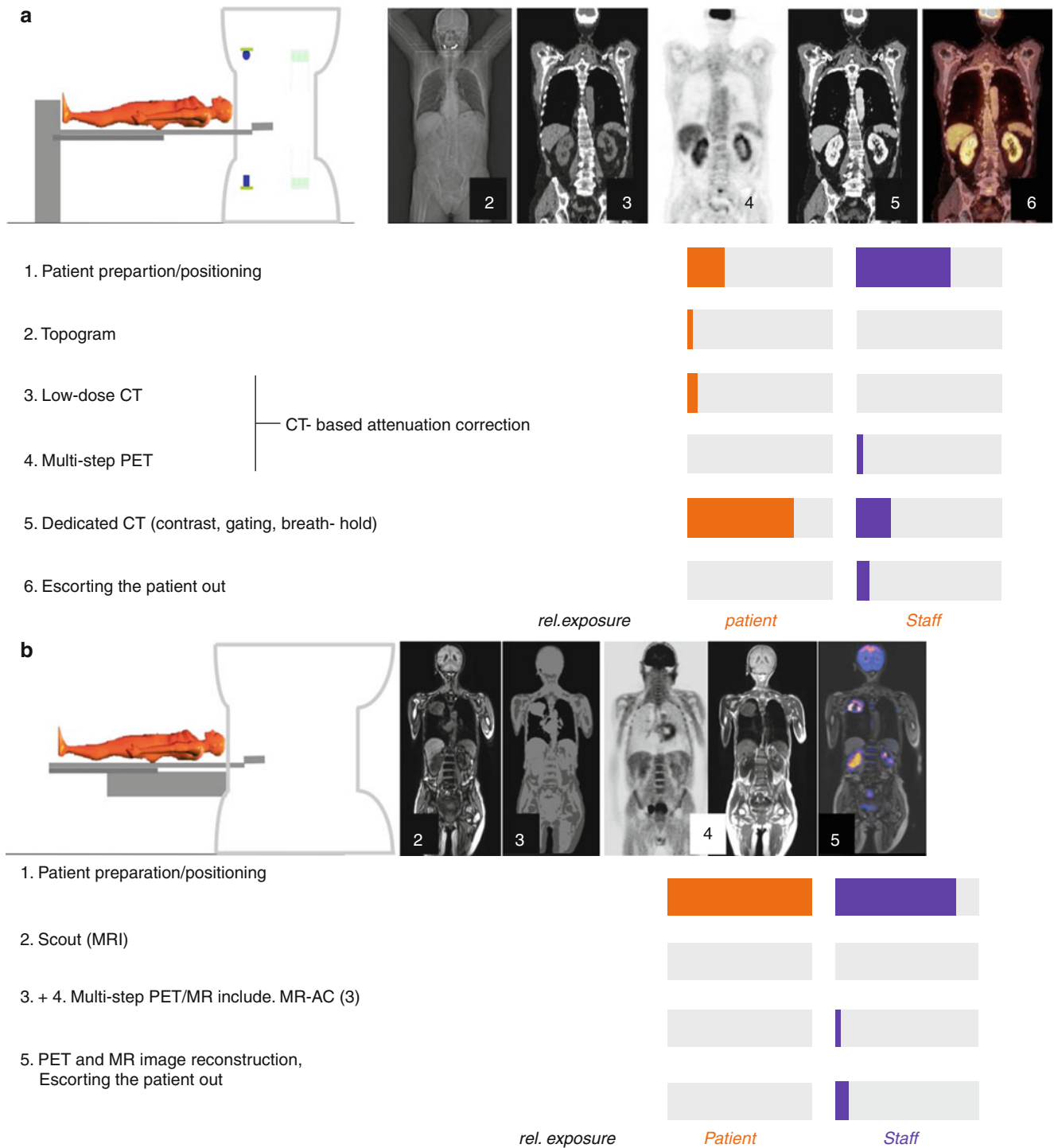


Fig. 2.15 Relative contributions to patient and staff exposure during a whole-body oncology examination in PET/CT (a) and PET/MR (b). The amount of radioactivity injected into the patient for a PET/CT (a, step 1) and PET/MR (a, step 1) is assumed to be identical. Note, patient

set-up in PET/MR is more elaborate and, therefore, relative and potentially total staff exposures are expected to be higher than those in PET/CT

Acknowledgement We are indebted to Gaspar Delso (GEHC), Hans Herzog (Research Centre Jülich), Jens-Christoph Georgi (Siemens Healthcare), Antonis Kalemis (Philips Healthcare), Bernd Pichler (University of Tübingen), Nina Schwenzer (University of Tübingen),

Jürgen Scheins (Research Centre Jülich), Holger Schmidt (University of Tübingen), David W Townsend (Singapore), Rainer Veigel (Philips Healthcare), Patrick Veit-Haibach (Zurich) for helpful discussions and the provision of support materials.

References

- Gambhir SS et al (2001) A tabulated summary of the FDG PET literature. *J Nucl Med* 42(5 suppl):1S–93S
- Herholz K, Heiss W-D (2004) Positron emission tomography in clinical neurology. *Mol Imaging Biol* 6(4):239–269
- Knuuti J (2004) Clinical cardiac PET in the future. *Eur J Nucl Med* 31(4):467–468
- Wahl RL et al (1993) “Anatomometabolic” tumor imaging: fusion of FDG PET with CT or MRI to localize foci of increased activity. *J Nucl Med* 34:1190–1197
- Wagner HN (1998) A brief history of positron emission tomography. *Semin Nucl Med* XXVIII(3):213–220
- Townsend D (2008) Multimodality imaging of structure and function. *Phys Med Biol* 53(4):R1–R39
- von Schulthess GK (2000) Cost considerations regarding an integrated CT-PET system. *Eur Radiol* 10(suppl 3):S377–S380
- Czernin J, Allen-Auerbach M, Schelbert H (2007) Improvements in cancer staging with PET/CT: literature-based evidence as of September 2006. *J Nucl Med* 48(1 suppl):78S–88S
- Lonsdale M, Beyer T (2010) Dual-modality PET/CT instrumentation-today and tomorrow. *Eur J Radiol* 73(3):452–460
- Kinahan P, Hasegawa B, Beyer T (2003) X-ray based attenuation correction for PET/CT scanners. *Semin Nucl Med* XXXIII(3):166–179
- von Schulthess GK, Steinert HC, Hany TF (2006) Integrated PET/CT: current applications and future directions. *Radiology* 238(2):405–422
- Kinahan PE et al (1998) Attenuation correction for a combined 3D PET/CT scanner. *Med Phys* 25(10):2046–2053
- Burger C et al (2002) PET attenuation coefficients from CT images: experimental evaluation of the transformation of CT into PET 511-keV attenuation coefficients. *Eur J Nucl Med* 29(7):922–927
- Beyer T et al (2000) A combined PET/CT tomograph for clinical oncology. *J Nucl Med* 41(8):1369–1379
- Beyer T et al (2011) The future of hybrid imaging – part 2: PET/CT. *Insights Imaging* 2(3):225–234
- Karp J et al (2008) Benefit of time-of-flight in PET: experimental and clinical results. *J Nucl Med* 49(3):462–470
- Jakoby B et al (2009) Performance characteristics of a new LSO PET/CT scanner with extended axial field-of-view and PSF reconstruction. *IEEE Trans Nucl Sci* 56(3):633–639
- Budinger T (1983) Time-of-flight positron emission tomography: status relative to conventional PET. *J Nucl Med* 24(1):73–78
- Kadrmas D et al (2009) Impact of time-of-flight on PET tumor detection. *J Nucl Med* 50(8):1315–1323
- Lois C et al (2010) An assessment of the impact of incorporating time-of-flight information into clinical PET/CT imaging. *J Nucl Med* 51(2):237–245
- Goffin K et al (2010) Anatomy-based reconstruction of FDG-PET images with implicit partial volume correction improves detection of hypometabolic regions in patients with epilepsy due to focal cortical dysplasia diagnosed on MRI. *Eur J Nucl Med Mol Imaging* 37(6):1148–1155
- Fletcher J et al (2008) Recommendations on the Use of 18F-FDG PET in oncology. *J Nucl Med* 49(3):480–508
- Pichler B et al (2010) PET/MRI: paving the way for the next generation of clinical multimodality imaging applications. *J Nucl Med* 51(3):333–336
- Wehrl H et al (2009) Pre-clinical PET/MR: technological advances and new perspectives in biomedical research. *Eur J Nucl Med Mol Imaging* 36(suppl 1):S56–S68
- Padhani A, Miles K (2010) Multiparametric imaging of tumor response to therapy. *Radiology* 256(2):348–364
- Moser E et al (2009) Magnetic resonance imaging methodology. *Eur J Nucl Med Mol Imaging* 36(suppl 1):S30–S41
- Porter D, Smith M (1988) Magnetic resonance spectroscopy in vivo. *J Biomed Eng* 10(6):562–568
- Bammer R (2003) Basic principles of diffusion-weighted imaging. *Eur J Radiol* 45(3):169–184
- Basser P et al (2000) In vivo fiber tractography using DT-MRI data. *Magn Reson Med* 44(4):625–632
- Golay X et al (2002) High-resolution isotropic 3D diffusion tensor imaging of the human brain. *Magn Reson Med* 47(5):837–843
- Padhani A, Koh D, Collins D (2011) Whole-body diffusion-weighted MR imaging in cancer: current status and research directions. *Radiology* 261(3):700–718
- Ogawa S et al (1993) Functional brain mapping by blood oxygenation level-dependent contrast magnetic resonance imaging. A comparison of signal characteristics with a biophysical model. *Biophys J* 64(3):803–812
- Sodickson D, Manning W (1997) Simultaneous acquisition of spatial harmonics (SMASH): fast imaging with radiofrequency coil arrays. *Magn Reson Med* 38(4):591–603
- Pruessmann K et al (1999) SENSE: sensitivity encoding for fast MRI. *Magn Reson Med* 42(5):952–962
- Griswold M et al (2002) Generalized autocalibrating partially parallel acquisitions (GRAPPA). *Magn Reson Med* 47(6):1202–1210
- Barkhausen J et al (2001) Whole-body MR imaging in 30 seconds with real-time true FISP and a continuously rolling table platform: feasibility study. *Radiology* 220(1):252–256
- Quick H et al (2004) High spatial resolution whole-body MR angiography featuring parallel imaging: initial experience. *Fortschr Roentgenstr* 176(2):163–169
- Veit-Haibach P et al (2013) PET/MR imaging using a Tri-modality PET/CT – MR system with a dedicated shuttle in clinical routine. *MAGMA* 26(1):25–35
- von Schulthess GK, Burger C (2010) Integrating imaging modalities: what makes sense from a workflow perspective? *Eur J Nucl Med Mol Imaging* 37(5):980–990
- Kalemis A, Delattre B, Heinzer S (2013) Sequential whole-body PET/MR scanner: concept, clinical use, and optimisation after two years in the clinic. The manufacturer’s perspective. *MAGMA* 26(1):5–23
- Zaidi H et al (2011) Design and performance evaluation of a whole-body Ingenuity TF PET/MRI system. *Phys Med Biol* 56(10):3091–3106
- Kalemis A, Delattre B, Heinzer S (2013) Sequential whole-body PET/MR scanner – concept, clinical use and optimisations after two years in the clinic. The manufacturer’s perspective. *MAGMA* 26(1):5–23
- Schmand M et al (2007) BrainPET: first human tomograph for simultaneous (functional) PET and MR imaging. *J Nucl Med* 48(6):45P
- Pichler B et al (2006) Performance test of an LSO-APD detector in a 7-T MRI scanner for simultaneous PET/MRI. *J Nucl Med* 47(4):639–647
- Herzog H et al (2010) The current state, challenges and perspectives of MR-PET. *Neuroimage* 49(3):2072–2082
- Schlemmer H et al (2008) Simultaneous MR/PET imaging of the human brain: feasibility study. *Radiology* 248(3):1028–1035
- Boss A et al (2010) Hybrid PET/MRI of intracranial masses: initial experiences and comparison to PET/CT. *J Nucl Med* 51(8):1198–1205
- Schwenzer N et al (2012) Simultaneous PET/MR imaging in a human brain PET/MR system in 50 patients-current state of image quality. *Eur J Radiol* 81(11):3472–3478
- Delso G et al (2011) Performance measurements of the Siemens mMR integrated whole-body PET/MR scanner. *J Nucl Med* 52(12):1914–1922
- Catana C et al (2011) MRI-assisted PET motion correction for neurologic studies in an integrated MR-PET scanner. *J Nucl Med* 52(1):154–161
- Tsoumpas C et al (2012) Fast generation of 4D PET/MR data from real dynamic MR acquisitions. *Phys Med Biol* 56(20):6597–6613

52. Truhn D, Kiessling F, Schulz V (2011) Optimized RF shielding techniques for simultaneous PET/MR. *Med Phys* 38(7):3995–4000
53. Hammer B (1990) NMR-PET scanner apparatus. U.S. Patent, USA, 3 July 1990
54. Lecomte R (2009) Novel detector technology for clinical PET. *Eur J Nucl Med Mol Imaging* 36(suppl 1):S69–S85
55. Degenhardt C et al (2009) The digital silicon photomultiplier — a novel sensor for the detection of scintillation light. In: IEEE nuclear science symposium conference (NSS/MIC), Orlando, 24 Oct–1 Nov 2009
56. Keereman V et al (2013) Challenges and current methods for attenuation correction in PET/MR. *MAGMA* 26(1):81–98
57. Zaidi H, Hasegawa B (2003) Determination of the attenuation map in emission tomography. *J Nucl Med* 44(2):291–315
58. Beyer T et al (2008) MR-based attenuation correction for torso-PET/MR imaging: pitfalls in mapping MR to CT data. *Eur J Nucl Med Mol Imaging* 35(6):1142–1146
59. Hofmann M et al (2009) Towards quantitative PET/MRI: a review of MR-based attenuation correction techniques. *Eur J Nucl Med Mol Imaging* 36(suppl 1):S93–S103
60. Hofmann M et al (2011) MRI-based attenuation correction for whole-body PET/MRI: quantitative evaluation of segmentation- and atlas-based methods. *J Nucl Med* 52(9):1392–1399
61. Martinez-Möller A et al (2009) Tissue classification as a potential approach for attenuation correction in whole-body PET/MRI: evaluation with PET/CT data. *J Nucl Med* 50(4):520–526
62. Delso G et al (2009) Study of MR head and neck coil for its use in an integrated MR/PET scanner. *J Nucl Med* 50(suppl 2):294–295P
63. Delso G et al (2010) Evaluation of the attenuation properties of MR equipment for its use in a whole-body PET/MR scanner. *Phys Med Biol* 55(15):4361–4374
64. Tellmann L et al (2011) The effect of MR coils on PET quantification in whole-body PET/MR: results from a pseudo-PET/MR phantom study. *Med Phys* 38(5):2795–2805
65. MacDonald L et al (2011) Effects of MR surface coils on PET quantification. *Med Phys* 38(6):2948–2953
66. Lois C et al (2011) Effect of MR contrast agents on quantitative accuracy of PET in combined whole-body PET/MR imaging. *Eur J Nucl Med Mol Imaging* 38(suppl 2):S156
67. Lee W et al (2011) Effects of MR contrast agents on PET quantification in PET/MRI study. *J Nucl Med* 52(suppl 1):53
68. Beyer T et al (2006) Whole-body 18F-FDG PET/CT in the presence of truncation artifacts. *J Nucl Med* 47(1):91–99
69. Delso G et al (2010) The effect of limited MR field of view in MR/PET attenuation correction. *Med Phys* 37(6):2804–2812
70. Nuyts J et al (1999) Simultaneous maximum a posteriori reconstruction of attenuation and activity distributions from emission sinograms. *IEEE Trans Med Imaging* 18(5):393–403
71. Salomon A et al (2009) Iterative generation of attenuation maps in TOF-PET/MR using consistency conditions. *J Nucl Med* 50(suppl 2):425P
72. Leahy R, Yan X (1991) Incorporation of anatomical MR data for improved functional imaging with PET. In: XIIth IPMI international conference, Wye, 1991
73. Lipinski B et al (1997) Expectation maximization reconstruction of positron emission tomography images using anatomical magnetic resonance information. *IEEE Trans Med Imaging* 16(2):129–136
74. Meltzer C et al (1990) Correction of PET data for partial volume effects in human cerebral cortex by MR imaging. *J Comput Assist Tomogr* 14(4):561
75. Meltzer CC et al (1999) Comparative evaluation of MR-based partial-volume correction schemes for PET. *J Nucl Med* 40(12):2053–2065
76. Beyer T et al (2003) A limited breath-hold technique for improved image quality in multi-slice PET/CT exams. *J Nucl Med* 44(5):274P–275P
77. Beyer T et al (2003) Dual-modality PET/CT imaging: the effect of respiratory motion on combined image quality in clinical oncology. *Eur J Nucl Med* 30(4):588–596
78. Nehmeh S et al (2007) Deep-inspiration breath-hold PET/CT of the thorax. *J Nucl Med* 48(1):22–26
79. Mori S et al (2009) Effective doses in four-dimensional computed tomography for lung radiotherapy planning. *Med Dosim* 34(1):87–90
80. Chang G et al (2010) Implementation of an automated respiratory amplitude gating technique for PET/CT: clinical evaluation. *J Nucl Med* 51(1):16–24
81. van der Kouwe A, Benner T, Dale A (2006) Real-time rigid body motion correction and shimming using cloverleaf navigators. *Magn Reson Med* 56(5):1019–1032
82. Kellman P et al (2008) Fully automatic, retrospective enhancement of real-time acquired cardiac cine MR images using image-based navigators and respiratory motion-corrected averaging. *Magn Reson Med* 59(4):771–778
83. Tsoumpas C et al (2010) Simultaneous PET/MR acquisition and MR-derived motion fields for correction of non-rigid motion in PET. *Ann Nucl Med* 24(10):745–750
84. King A et al (2012) Thoracic respiratory motion estimation from MRI using a statistical model and a 2-D image navigator. *Med Imaging Anal* 16(1):252–264
85. Buerger C et al (2012) Nonrigid motion modeling of the liver from 3-D undersampled self-gated golden-radial phase encoded MRI. *IEEE Trans Med Imaging* 31(3):805–815
86. Brix G et al (2005) Radiation exposure of patients undergoing whole-body dual-modality FDG-PET/CT examinations. *J Nucl Med* 46(4):608–613
87. Brix G et al (2009) Risks and safety aspects related to PET/MR examinations. *Eur J Nucl Med Mol Imaging* 36(suppl 1):S131–S138
88. Goyen M, Debatin J (2009) Healthcare costs for new technologies. *Eur J Nucl Med Mol Imaging* 36(suppl 1):S139–S143